VOLUME 32 MARCH 1954 NUMBER 3

Canadian Journal of Physics

Editor: G. M. VOLKOFF

Associate Editors:

L. G. ELLIOTT, *Atomic Energy of Canada, Ltd., Chalk River*
J. S. FOSTER, *McGill University*
G. HERZBERG, *National Research Council of Canada*
L. LEPRINCE-RINGUET, *Ecole Polytechnique, Paris*
D. W. R. McKINLEY, *National Research Council of Canada*
B. W. SARGENT, *Queen's University*
F. E. SIMON, *Clarendon Laboratory, University of Oxford*
W. H. WATSON, *University of Toronto*

Published by THE NATIONAL RESEARCH COUNCIL

OTTAWA CANADA

CANADIAN JOURNAL OF PHYSICS

(Formerly Section A, Canadian Journal of Research)

The CANADIAN JOURNAL OF PHYSICS is published monthly by the National Research Council of Canada under the authority of the Chairman of the Committee of the Privy Council on Scientific and Industrial Research. The National Research Council publishes also: *Canadian Journal of Biochemistry and Physiology, Canadian Journal of Botany, Canadian Journal of Chemistry, Canadian Journal of Technology, Canadian Journal of Zoology.*

Matters of general policy concerning the Council's journals are the responsibility of a joint Editorial Board consisting of: the Editors of the journals; members representing the National Research Council of Canada and the Royal Society of Canada and three other scientific societies; and two ex-officio members.

EDITORIAL BOARD

Editors of the Journals

D. L. Bailey, *University of Toronto*
J. B. Collip, *University of Western Ontario*
E. H. Craigie, *University of Toronto*
G. A. Ledingham, *National Research Council*
Léo Marion, *National Research Council*
G. M. Volkoff, *University of British Columbia*

Representatives of the National Research Council

C. W. Argue (Chairman), *University of New Brunswick*
G. E. Hall, *University of Western Ontario*
T. Thorvaldson, *University of Saskatchewan*
W. H. Watson, *University of Toronto*

Representatives of Societies

D. L. Bailey, *University of Toronto*
Royal Society of Canada
J. B. Collip, *University of Western Ontario*
Canadian Physiological Society
E. H. Craigie, *University of Toronto*
Royal Society of Canada
H. G. Thode, *McMaster University*
Chemical Institute of Canada
T. Thorvaldson, *University of Saskatchewan*
Royal Society of Canada
G. M. Volkoff, *University of British Columbia*
Royal Society of Canada
Canadian Association of Physicists

Ex officio

Léo Marion (Editor-in-Chief)
National Research Council
H. H. Saunderson
National Research Council

Manuscripts should be addressed to:

Dr. Léo Marion,
Editor-in-Chief,
Canadian Journal of Physics,
National Research Council,
Ottawa 2, Canada.

Subscriptions, renewals, and orders for back numbers should be addressed to:

Division of Administration,
National Research Council,
Ottawa 2, Canada.

Subscription rate: $4.00 a year, single numbers: 75 cents. Remittances should be made payable to the Receiver General of Canada, credit National Research Council.

Canadian Journal of Physics

Issued by THE NATIONAL RESEARCH COUNCIL OF CANADA

VOLUME 32 MARCH 1954 NUMBER 3

THE IMPEDANCE OF AN ANTENNA ABOVE A CIRCULAR GROUND PLATE LAID UPON A PLANE EARTH[1]

BY G. BEKEFI

ABSTRACT

Recent theoretical work by Storer, concerning the impedance of a vertical antenna in contact with a circular metal disk, is extended to include the case when the system is laid upon an imperfectly conducting plane earth. The expression for the impedance of the antenna is cast into a form which is stationary with respect to small variations (about the true value) of the unknown radial electric field over the surface of the earth. Numerical results are given for the case when the ground plate is sufficiently large as compared to the wave length of the radiation; the effect of variations in dielectric constant of the earth upon the impedance is shown. These calculations are compared to those obtained from the approximate theory of Monteath.

A second variational formula for the antenna impedance is developed in terms of surface currents flowing in the metal ground plate. The application of this method becomes useful when the ground plate is not too large in comparison with the wave length.

1. INTRODUCTION

The problem of determining the impedance and the radiation pattern of a thin wire antenna erected vertically at the center of a circular metal ground plate has received considerable attention, both theoretical and experimental. Theoretically, it is a case of diffraction of a very special type, belonging to that class of problems in electromagnetic theory which are reducible to a solution of the scalar wave equation. As early as 1930 Bardeen (2) attempted to solve this problem but he was successful only in the case when the disk is small with respect to the wave length of the radiation. Leitner and Spence (7) were able to extend this range by separating the wave equation in spheroidal co-ordinates. Their calculations compare favorably with measurements performed by Meier and Summers (10). However when the disk is excessively large, difficulties are experienced with the slow convergence of their infinite series. Recently, with the aid of Levine and Schwinger's (8) variational principle, Storer (16) was able to calculate the impedance and radiation pattern of an antenna over a very large ground plate.

A problem of considerable practical interest is one in which the disk is allowed to rest on the surface of a partially conducting plane earth, rather than it being assumed to be isolated in free space as was done by the above-mentioned

[1] *Manuscript received October 27, 1953.*
Contribution from the Eaton Electronics Research Laboratory, Department of Physics, McGill University, Montreal, Canada.

workers. Practical construction design data of a ground system consisting of radial wires (thus simulating a solid circular disk) have been proposed by Abbott (1) and Brown and collaborators (5).

To this author's knowledge no attempt has been made as yet to formulate this problem subject to exact boundary conditions. The only work available is an approximate theory by Monteath (12) which was later applied to a variety of cases by Surtees (18).

This paper is concerned mainly with the above problem, namely to calculate the impedance of an antenna above a circular ground plate resting upon a flat, partially conducting earth. To this purpose an integral equation is developed for the radial electric field which exists over the surface of the earth. By a method similar to that given by Storer, the expression for the impedance is thrown into a variational form and by a suitable choice of trial function for the radial electric field (dependent upon the properties of the ground), the desired result is obtained. The dependence of the trial function and of the impedance upon the dielectric constant of the earth is discussed. A comparison of calculations thus obtained with those based on the theory of Monteath shows satisfactory agreement.

Although the variational formulation developed by Storer fulfills its purpose when the ground plate is large as compared to the wave length, it is not well suited for small disks or disks of the order of several wave lengths in diameter. The last part of this paper describes an alternate variational formula better suited to this range of wave lengths, given in terms of the radial currents flowing in the disk. The two variational formulae are in a sense complementary and together they cover a large range of wave lengths.

2. GENERAL FORMULATION OF PROBLEM

The system under consideration is shown in Fig. 1. A thin perfectly conducting metal disk of radius a is laid upon a flat imperfectly conducting earth of dielectric

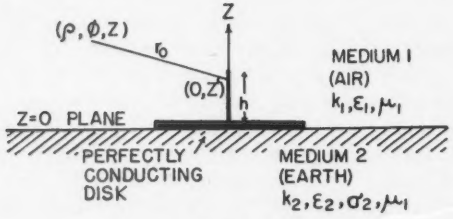

FIG. 1.

constant ϵ_2 and conductivity σ_2. A thin wire antenna of length h is erected vertically at the center of the disk with the input terminals at its base. The emitted radiation is assumed to vary sinusoidally in time as exp $(-j\omega t)$ where ω is the angular frequency. The m.k.s. system of units is used throughout. Cylindrical co-ordinates (ρ, ϕ, z) are used with the z co-ordinate coincident with the axis of the antenna.

The radiation in space will be represented by the Hertz vector $\mathbf{\Pi}$ from which

the electric and magnetic field components **E** and **H** are derived through the relations

$$\mathbf{E} = k^2\boldsymbol{\Pi} + \nabla\nabla\cdot\boldsymbol{\Pi}, \tag{1a}$$

$$\mathbf{H} = \frac{k^2}{j\omega\mu}\nabla\times\boldsymbol{\Pi}. \tag{1b}$$

Here k is the propagation constant and μ the magnetic permeability. Owing to the circular symmetry that exists in the geometry of the diffracting system, the field components are independent of the ϕ co-ordinate and the radiation at any point in space can be represented by the z component of the Hertz vector alone, namely Π_z, with $\Pi_x = \Pi_y = 0$. For convenience a quantity U is defined by

$$U = \partial\Pi_z/\partial\rho$$

in terms of which the field components as given by Equations [1a, b] are

$$\begin{aligned} &(a)\ E_\rho = \partial U/\partial z, && (c)\ H_\phi = -\frac{k^2}{j\omega\mu}U, \\ &(b)\ E_z = -\frac{1}{\rho}\frac{\partial}{\partial\rho}(\rho U), && (d)\ E_\phi = H_\rho = H_z = 0. \end{aligned} \tag{2}$$

The final solution must furthermore satisfy the homogeneous scalar wave equation

$$\nabla^2\Pi_z + k^2\Pi_z = 0. \tag{3}$$

The total wave function U will now be split up into an incident field U^i that is associated with the antenna when this is assumed to be radiating in free space; a component U^r, the image of U^i in the plane $z = 0$, associated with a wave reflected by a perfectly conducting ground; and a "scattered" component U^s resulting from diffraction by the disk and the presence of the ground. Hence in medium 1,

$$U_1 = U_1^i + U_1^r + U_1^s, \qquad z \geqslant 0 \tag{4a}$$

while in medium 2 which is free from real sources, only the "scattered" component exists,

$$U_2 = U_2^s, \qquad z \leqslant 0. \tag{4b}$$

By requiring that E_ρ vanish over the area of the perfectly conducting disk and that the components of **E** and **H** tangential to the ground be continuous across the surface of the earth, the following boundary conditions are found from Equations [2]. (Following the assumption that is usually made, the earth's magnetic permeability is taken as equal to the free space value (μ_1). However, the theory may be developed free from this restriction.)

$$\partial U_1/\partial z = \partial U_2/\partial z = 0 \qquad \text{over disk} \tag{5a}$$

$$\left.\begin{aligned} \partial U_1/\partial z &= \partial U_2/\partial z \\ U_1 &= n^2 U_2 \end{aligned}\right\} \qquad \text{over earth} \tag{5b, 5c}$$

The symbol n denotes the complex refractive index which is given by

$$n = k_2/k_1 = [(\epsilon_2 + j\sigma_2/\omega)/\epsilon_1]^{\frac{1}{2}} \tag{6}$$

with k_1 as the free space propagation constant, 2π/wave length; ϵ_2 and σ_2 are the dielectric constant and conductivity of the earth respectively.

The well-known solution of the scalar wave equation [3] independent of the ϕ co-ordinate is given by (15)

$$[7] \qquad \Pi_z^s(\rho, z) = \int_0^\infty J_0(\lambda\rho)\, F(\lambda) \exp(\pm\alpha z) \frac{\lambda d\lambda}{\alpha}$$

where $J_0(x)$ is a Bessel function of order zero, λ is a variable of integration, and $F(\lambda)$ is any function of λ subject to the requirement that the field behave properly at infinity as stipulated by Sommerfeld's radiation conditions. The function α is defined as

$$\begin{aligned} \alpha &= (\lambda^2 - k^2)^{\frac{1}{2}}, \qquad \lambda > k, \\ &= -j(k^2 - \lambda^2)^{\frac{1}{2}}, \quad \lambda < k. \end{aligned}$$

In the exponent of Equation [7] the positive sign must be taken when $z < 0$, the negative sign when $z > 0$.

A differentiation of [7] with respect to ρ results in expressions for U^s, one for each of the two media,

$$[8a] \qquad U_1^s(\rho, z) = -\int_0^\infty J_1(\lambda\rho)\, F_1(\lambda) \exp(-\alpha_1 z) \frac{\lambda^2 d\lambda}{\alpha_1}, \quad \alpha_1 = (\lambda^2 - k_1^2)^{\frac{1}{2}},$$

$$[8b] \qquad U_2^s(\rho, z) = -\int_0^\infty J_1(\lambda\rho)\, F_2(\lambda) \exp(+\alpha_2 z) \frac{\lambda^2 d\lambda}{\alpha_2}, \quad \alpha_2 = (\lambda^2 - k_2^2)^{\frac{1}{2}}.$$

With the aid of Equations [8] and boundary conditions [5] the required integral equation will be obtained. On substituting [8*a*, *b*] into [4*a*, *b*] respectively and with recourse to conditions [5*a*, *b*] it follows that

$$[9a] \qquad F_1(\lambda) + F_2(\lambda) = 0, \qquad z = 0$$

and from [5*c*] that over the surface of the earth

$$[9b] \qquad 2U_1^i(\rho, 0) = \int_0^\infty J_1(\lambda\rho)[F_1(\lambda)/\alpha_1 - n^2 F_2(\lambda)/\alpha_2]\, \lambda^2 d\lambda, \qquad \rho > a.$$

Eliminating F_2 by substituting [9*a*] into [9*b*] results in

$$[10] \qquad 2U_1^i(\rho, 0) = \int_0^\infty J_1(\lambda\rho)\, F_1(\lambda)[1/\alpha_1 + n^2/\alpha_2]\, \lambda^2 d\lambda, \qquad \rho > a.$$

Equation [10] is a condition imposed on $F_1(\lambda)$ by boundary requirements over the earth's surface. The other requirement which will now be obtained is the vanishing of E_ρ over the surface of the disk. Since $\partial U_1^i/\partial z = -\partial U_1^r/\partial z$, it follows from [4*a*] and [8*a*] that at $z = 0$

$$[11] \qquad \partial U_1/\partial z = \int_0^\infty J_1(\lambda\rho)\, F_1(\lambda)\, \lambda^2 d\lambda.$$

A Fourier-Bessel transform of [11] yields

$$[12] \qquad \lambda F_1(\lambda) = \int_a^\infty J_1(\lambda\rho') \left(\frac{\partial U_1(\rho')}{\partial z}\right) \rho'\, d\rho'$$

where the integral extending from 0 to a vanishes because of [5*a*]. The quantity

$\partial U_1(\rho)/\partial z$ is the tangential component of the electric field over the surface of the earth; for convenience it will be denoted by $\xi(\rho)$. Eliminating $F_1(\lambda)$ from [10] by a substitution of [12], and defining $G(\rho, \rho')$, a Green's function at $z = 0$, by

$$[13] \qquad G(\rho, \rho') = \tfrac{1}{2} \int_0^\infty J_1(\lambda\rho)\, J_1(\lambda\rho')[1/\alpha_1 + n^2/\alpha_2]\, \lambda d\lambda,$$

it follows that

$$[14] \qquad U_1^i(\rho) = \int_a^\infty G(\rho, \rho')\, \xi(\rho')\, \rho'\, d\rho', \qquad z = 0^+.$$

If it were possible to solve the integral equation [14] for $\xi(\rho)$ (for any given value of the refractive index n), the field at any point in space could be determined by first finding $F_1(\lambda)$ from [12] and then calculating U_1^s. Finally the impedance of the antenna could be found by integrating Poynting's vector over a closed surface surrounding the radiator. Owing to the very complicated form of the integral equation, such a procedure however is not available. For that reason the expression for the impedance is put into a variational form and by a suitable choice of trial function for $\xi(\rho)$ the impedance is calculated without the necessity of solving the integral equation explicitly. It should be noted that on setting the refractive index of the earth equal to unity, we are led to Storer's problem of an antenna above a disk situated in free space. The corresponding integral equations can then be shown to be identical.

3. FIRST VARIATIONAL FORMULATION

It can be proved in general that the input impedance Z of a wire antenna referred to the maximum current amplitude $I(0)$ is given by (16, 14)

$$Z\, I(0)\, I^*(0) = -\lim_{\rho \to 0} \int_0^h E_z(\rho, z')\, I^*(z')\, dz'$$

where $I(z')$ is the current distribution over the length of the antenna and E_z is the electric field over its surface and tangential to its axis. The asterisks signify complex conjugates. Subdividing E_z in a manner analogous to [4a], the impedance can be written as

$$Z\, I(0)\, I^*(0) = -\lim_{\rho \to 0} \int_0^h [E_z^i(\rho, z') + E_z^r(\rho, z')]\, I^*(z')\, dz' - \lim_{\rho \to 0} \int_0^h E_z^s(\rho, z')\, I^*(z')\, dz'.$$

The first integral represents a contribution to the total impedance equal to that associated with the antenna placed over a perfectly conducting ground. Let us define ΔZ as the actual impedance of the antenna above a circular ground plate laid upon a partially conducting ground, minus the impedance the antenna would have over a perfectly conducting ground. It then follows from the above equation that

$$[15] \qquad \Delta Z\, I(0)\, I^*(0) = -\lim_{\rho \to 0} \int_0^h E_z^s(\rho, z')\, I^*(z')\, dz'.$$

Throughout the remainder of this paper, the idealized case of a sinusoidal current distribution over the antenna will be assumed of the form*

$$I(z') = I(0)\, K(z')$$

with $$K(z') = \sin k_1(h - z')/\sin k_1 h.$$

Hence equation [15] becomes

$$[16] \qquad \Delta Z\, I(0) = -\lim_{\rho \to 0} \int_0^h E_z^s(\rho, z')\, K(z')\, dz'.$$

The field component E_z^s will be written now as a function of $\xi(\rho)$, the radial electric field over the earth's surface. From equations [2*b*] and [8*a*] it is seen that

$$E_z^s(\rho, z') = -\frac{1}{\rho}\frac{\partial}{\partial \rho}[\rho U_1^s(\rho, z')]$$

$$= \frac{1}{\rho}\frac{\partial}{\partial \rho}\rho \int_0^\infty J_1(\lambda\rho)\, F_1(\lambda) \exp(-\alpha_1 z')\, \frac{\lambda^2 d\lambda}{\alpha_1}.$$

Substituting for $F_1(\lambda)$ from Equation [12] and proceeding to the limit $\rho \to 0$,

$$\lim_{\rho \to 0} E_z^s(\rho, z') = \int_0^\infty \exp(-\alpha_1 z')\, \frac{\lambda^2 d\lambda}{\alpha_1} \int_a^\infty J_1(\lambda\rho')\, \xi(\rho')\, \rho'\, d\rho'.$$

Inserting this expression into [16] gives

$$[17] \qquad \Delta Z\, I(0) = -\int_0^h K(z')\, dz' \int_0^\infty \exp(-\alpha_1 z')\, \frac{\lambda^2 d\lambda}{\alpha_1} \int_a^\infty J_1(\lambda\rho')\, \xi(\rho')\, \rho'\, d\rho'.$$

Considerable simplification of [17] results by identifying certain integrals with the value of U^i over the plane $z = 0$. For that purpose the explicit form of U^i will now be found.

The expression for the Hertz vector which describes the field of an antenna in free space is (17)

$$\Pi_z^i(\rho', z, z') = \frac{j}{4\pi\omega\epsilon_1} \int_0^h I(z')\, \frac{\exp(jk_1 r_0)}{r_0}\, dz', \qquad r_0^2 = \rho'^2 + (z - z')^2$$

and hence over the plane $z = 0$,

$$[18] \qquad U_1^i(\rho', z') = \frac{jI(0)}{4\pi\omega\epsilon_1}\frac{\partial}{\partial \rho} \int_0^h K(z')\, \frac{\exp(jk_1 r)}{r}\, dz', \quad r^2 = \rho'^2 + z'^2.$$

Using the well-known identity (15)

$$\frac{\exp(jk_1 r)}{r} = \int_0^\infty J_0(\lambda\rho') \exp(-\alpha_1 z')\, \frac{\lambda d\lambda}{\alpha_1},$$

it follows that

$$U_1^i(\rho', z') = \frac{-jI(0)}{4\pi\omega\epsilon_1} \int_0^h K(z')\, dz' \int_0^\infty J_1(\lambda\rho') \exp(-\alpha_1 z')\, \frac{\lambda^2 d\lambda}{\alpha_1}.$$

**To within a good degree of accuracy a sinusoidal current distribution is obtained in practice, either by making the antenna sufficiently thin and from material of high conductivity, or in cases of fairly thick antennas, provided that $kh \leq 0.75$. If these criteria cannot be met, $I(z')$ can be calculated by one of the methods outlined by Schelkunoff (Ref. 14, chapter 5).*

In consequence, Equation [17] becomes

$$[19] \qquad \frac{jI^2(0)}{4\pi\omega\epsilon_1}\,\Delta Z = \int_a^\infty U_1^i(\rho', z')\,\xi(\rho')\,\rho'\,d\rho'.$$

Finally an expression has been obtained for ΔZ in terms of U^i and the unknown $\xi(\rho)$.

Multiply both sides of the integral equation [14] by $\rho\xi(\rho)$ and integrate from a to ∞; then,

$$[20] \qquad \int_a^\infty U_1^i(\rho)\,\xi(\rho)\,\rho\,d\rho = \int_a^\infty \int_a^\infty G(\rho, \rho')\,\xi(\rho)\,\xi(\rho')\,\rho\,\rho'\,d\rho\,d\rho'.$$

It will be noted that because of the symmetry of the Green's function [13] in the co-ordinates ρ and ρ', an integral equation identical to that given by [20] is obtained on interchanging ρ and ρ'. A comparison of [19] with [20] shows that

$$[21] \qquad \frac{jI^2(0)}{4\pi\omega\epsilon_1}\,\Delta Z = \int_a^\infty \int_a^\infty G(\rho, \rho')\,\xi(\rho)\,\xi(\rho')\,\rho\,\rho'\,d\rho\,d\rho'.$$

Multiplying both sides of [21] by ΔZ and making use of relation [19], it is found that

$$[22] \qquad \frac{jI^2(0)}{4\pi\omega\epsilon_1}\,\Delta Z = \frac{\left[\int_a^\infty U_1^i(\rho', z')\,\xi(\rho')\,\rho'\,d\rho'\right]^2}{\int_a^\infty \int_a^\infty G(\rho, \rho')\,\xi(\rho)\,\xi(\rho')\,\rho\,\rho'\,d\rho\,d\rho'}$$

which is the required variational form for the antenna impedance. It can be shown that a small variation $\delta(\Delta Z)$ produced by small variations in $\xi(\rho)$ and $\xi(\rho')$ about their correct values as given by [20] makes $\delta(\Delta Z) = 0$. Conversely, if ΔZ given by [22] is stationary, then $\xi(\rho)$ must satisfy the integral equation [20]. The evaluation of [22] is effected by choosing a trial function for $\xi(\rho)$ containing a sufficient number of arbitrary coefficients which are then determined by invoking the stationary property of ΔZ. This will be done in the next section for the special case of a disk which is assumed large as compared to the wave length. The procedure adopted will be very similar to that described by Storer.

4. SPECIAL CASE OF A LARGE GROUND PLATE

The numerical evaluation of [22] is greatly facilitated by assuming $k_1 a \gg 1$ and $k_1 a \gg k_1 h$. Under these conditions the expression for U_1^i given by [18] approximates to

$$[23] \qquad U_1^i(\rho', z') \doteqdot \frac{jI(0)}{4\pi\omega\epsilon_1}\,\frac{\partial}{\partial\rho}\left(\frac{\exp(jk_1\rho)}{\rho}\right)\int_0^h K(z')\,dz'$$

$$\doteqdot -\frac{\eta_0 I(0)}{4\pi}\,\frac{\exp(jk_1\rho)}{\rho}\int_0^h K(z')\,dz'$$

where η_0 is the free space impedance $(\mu_1/\epsilon_1)^{\frac{1}{2}} = 120\pi$ ohms. Inserting this value of U^i into [22] yields

$$[24] \qquad \Delta Z = \frac{k_1\eta_0}{4\pi j} \frac{\left[\int_0^h K(z')\,dz'\right]^2 \left[\int_a^\infty \exp(jk_1\rho)\,\xi(\rho)\,d\rho\right]^2}{\int_a^\infty \int_a^\infty G(\rho, \rho')\,\xi(\rho)\,\xi(\rho')\,\rho\,\rho'\,d\rho\,d\rho'}.$$

The Green's function $G(\rho, \rho')$ given by Equation [13] can be evaluated by replacing the Bessel functions in its integrand by their asymptotic values (16) (since $k_1\rho$ and $k_1\rho' \gg 1$). This gives the following expression for $G(\rho, \rho')$:

$$[25] \quad G(\rho, \rho') = \frac{j}{4(\rho\rho')^{\frac{1}{2}}} [H_0^{(1)}(k_1|\rho - \rho'|) + n^2 H_0^{(1)}(k_2|\rho - \rho'|)], \qquad ka \gg 1$$

where $H_0^{(1)}$ is a Hankel function of order zero.

A simple form of a trial function for $\xi(\rho)$ is

$$[26] \qquad \xi(\rho) = \frac{\exp(jk_1\rho f)}{\rho^{3/2}(\rho - a)^{\frac{1}{2}}}.$$

This function falls off with ρ rapidly enough to ensure integrability over the whole plane $z = 0$ and it also exhibits a singularity at $\rho = a$ of the correct order, as required by the edge conditions of Bouwkamp (3) and Meixner (11). The exponential term signifies an outwardly directed wave, travelling over the earth's surface and having a propagation constant equal to $(k_1 f)$; the as yet unknown quantity f is a function of the complex refractive index, n, of the earth.

Substituting the trial function [26] into the equation for the impedance [24], it is found that

$$[27] \qquad \Delta Z = \frac{k_1\eta_0}{4\pi j}\left[\int_0^h K(z')\,dz'\right]^2 (T_1)^2/T_2$$

where
$$T_1 = \int_a^\infty \frac{\exp(jk_1\rho[1 + f])}{\rho^{3/2}(\rho - a)^{\frac{1}{2}}}\,d\rho,$$

$$T_2 = \int_a^\infty \int_a^\infty G(\rho, \rho') \frac{\exp(jk_1 f[\rho + \rho'])}{(\rho\rho')^{\frac{1}{2}}(\rho - a)^{\frac{1}{2}}(\rho' - a)^{\frac{1}{2}}}\,d\rho\,d\rho'.$$

By partial integration T_1 can be transformed into

$$T_1 = \left[-x^{-3/2}\int_x^\infty \frac{\exp(jk_1\rho[1 + f])}{(\rho - a)^{\frac{1}{2}}}\,d\rho\right]_a^\infty + \frac{3}{2}\int_a^\infty \int_x^\infty \frac{\exp(jk_1\rho[1+f])}{(\rho - a)^{\frac{1}{2}}}\,d\rho x^{-5/2}dx.$$

For very large values of k_1a, the second integral can be neglected in comparison with the first, as it is one order smaller in (k_1a). Hence,

$$T_1 = a^{-3/2}\int_a^\infty \frac{\exp(jk_1\rho[1 + f])}{(\rho - a)^{\frac{1}{2}}}\,d\rho$$

$$[28a] \qquad = a^{-3/2}\exp(jk_1a[1 + f])\int_0^\infty \exp(jk_1t[1 + f])\frac{dt}{t^{\frac{1}{2}}}$$

$$= \left\{\frac{\pi}{k_1a^3(1 + f)}\right\}^{\frac{1}{2}} \exp(jk_1a[1 + f] + j\pi/4) + O(a^{-5/2}).$$

By a similar procedure it can be shown that

$$[28b] \qquad T_2 = a^{-2} \int_a^\infty \int_a^\infty G(\rho, \rho') \frac{\exp\,(jk_1 f[\rho + \rho'])}{(\rho - a)^{\frac{1}{2}}(\rho' - a)^{\frac{1}{2}}} (\rho\rho')^{\frac{1}{2}}\, d\rho\, d\rho' + O(a^{-3}).$$

On substituting for $G(\rho, \rho')$ from [25] and making a change of variable, $x = (\rho - a)$, $x' = (\rho' - a)$, T_2 becomes

$$[29] \qquad T_2 = \frac{j \exp\,(2jk_1 af)}{4a^2} \left\{ \int_0^\infty \int_0^\infty H_0^{(1)}(k_1|x - x'|) \frac{\exp\,(jk_1 f[x + x'])}{(xx')^{\frac{1}{2}}}\, dx\, dx' \right.$$

$$\left. + n^2 \int_0^\infty \int_0^\infty H_0^{(1)}(k_2|x - x'|) \frac{\exp\,(jk_1 f[x + x'])}{(xx')^{\frac{1}{2}}}\, dx\, dx' \right\}.$$

The double integrals appearing in [29] can be simplified by following the method employed by Storer. Setting $u = x - x'$ and $v = x + x'$, rotating the coordinates, and using the integral representation

$$H_0^{(1)}(z) = \frac{2}{\pi j} \int_0^\infty \exp\,(jz \cosh \theta)\, d\theta,$$

the double integrals (which will be denoted by B_1 and B_2 respectively) become

$$[30a] \qquad B_1 = \frac{j\pi}{k_1} \int_0^\infty H_0^{(1)}(y)\, H_0^{(1)}(fy)\, dy,$$

$$[30b] \qquad B_2 = \frac{j\pi}{k_1} \int_0^\infty H_0^{(1)}(ny)\, H_0^{(1)}(fy)\, dy,$$

so that

$$T_2 = \frac{j \exp\,(2jk_1 af)}{4a^2} [B_1 + n^2 B_2].$$

Inserting the values of T_1 and T_2 into [27] gives the following result for ΔZ:

$$[31] \qquad \Delta Z = \frac{\eta_0 \exp\,(2jk_1 a)}{j(k_1 a)} \frac{[k_1 \int_0^h K(z')\, dz']^2}{k_1(1+f)(B_1 + n^2 B_2)}, \qquad k_1 a \gg 1$$

where B_1 and B_2 are defined by [30a, b]. In the above equation for the impedance the only unknown which must be determined is the value of f as a function of the refractive index n. This is done by invoking the stationary character of ΔZ; namely those values f_s of f are required which satisfy

$$d(\Delta Z)/df = 0,$$

and from [31], this is equivalent to saying that f must satisfy the differential equation

$$[32] \qquad (1 + f) = -(B_1 + n^2 B_2)/d(B_1 + n^2 B_2)/df.$$

Owing to the rather lengthy computational work which is involved in finding a solution of [32], only the case when n is real will be considered. This applies when the ratio of conductivity/signal frequency can be neglected as compared to the dielectric constant of the earth (see Equation [6]). This state of affairs occurs for instance when the earth is very hard and dry and when the frequency is sufficiently high. A typical case is (18), $\epsilon_2/\epsilon_1 \sim 5$, $\sigma_2 \sim 2 \times 10^{-4}$ mhos/meter, $\omega \sim 2\pi \times 10^7$ c./s., and leads to $n \sim (2.24 + j\,0.08)$.

A solution of [32] for f requires an evaluation of the integrals B_1 and B_2. A

method of obtaining a solution in the form of an infinite series is outlined in the Appendix. The integrals B_1 and B_2 are seen to be of the type

$$[33a] \qquad k_1 B(a, b) = j\pi \int_0^\infty H_0^{(1)}(ay)\, H_0^{(1)}(by)\, dy, \qquad a, b > 0.$$

As shown in the Appendix, [33a] becomes

$$[33b] \quad k_1 B(a, b) = -\frac{2}{\pi b} \sum_{r=0}^{\infty} \frac{\Gamma^2(r + \frac{1}{2})}{(r!)^2} \left(\frac{a}{b}\right)^{2r} \left[\ln\left(\frac{a}{b}\right) + \psi(r + \tfrac{1}{2}) - \psi(r+1)\right]$$

for $b > a$; if $b < a$ the roles of a and b must be interchanged. The functions $\psi(r + \frac{1}{2}), \psi(r + 1)$ are defined as (9)

$$\psi(z) = \frac{d \ln \Gamma(z)}{dz}.$$

The above series diverges when $a = b$; in this case it can be shown (16) that

$$[33c] \qquad k_1 B(a, a) = \pi/a.$$

The series for B_1 and B_2 were substituted into [34] and the differentiation with respect to f was then performed; the resultant equation was solved by a graphical method. For a given value of n the right-hand side of [32] was plotted as a function of f and the point of intersection of this curve with the straight line $(1 + f)$ gave the value of f_s that makes ΔZ stationary. The results of the calculations are shown in Fig. 2 where f_s is plotted as a function of n. In view

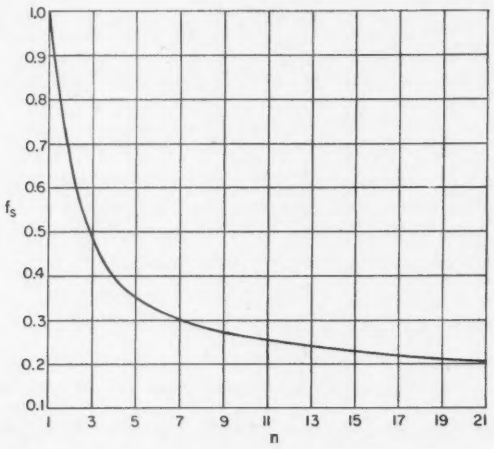

FIG. 2. Variation of the propagation constant of the surface wave (f_s) with the earth's refractive index (n).

of the fact that $(k_1 f_s)$ represents the propagation constant of $\xi(\rho)$, the surface wave travelling over the earth, the functional dependence of f_s upon n is of some interest. The rapid fall off of f_s caused by a small departure of n from unity should be noted. These results and also those that would be obtained for f_s

when n is complex invite further study in the light of surface wave propagation as predicted by Sommerfeld (15), Norton (13), and others.

Once f_s has been found for a given value of n, B_1 and B_2 are obtained from the series [33b] and can then be substituted into the expression [31] for the input impedance. In the special case $n = 1$, the problem is that of an antenna and ground plate situated in free space; under these conditions $f_s = 1$, $B_1 = B_2 = \pi/k_1$ (see Equation [33c]), and the impedance (denoted by the subscript F) becomes

$$[34] \qquad \Delta Z_F = \frac{\eta_0 \exp(2jk_1a)}{4\pi j(k_1a)} \left[k_1 \int_0^h K(z')\, dz' \right]^2$$

which is the formula obtained by Storer.

The variation of impedance with n is depicted in Fig. 3; along the ordinate is plotted the ratio $(\Delta Z/\Delta Z_F)$. The dashed line represents calculations that were

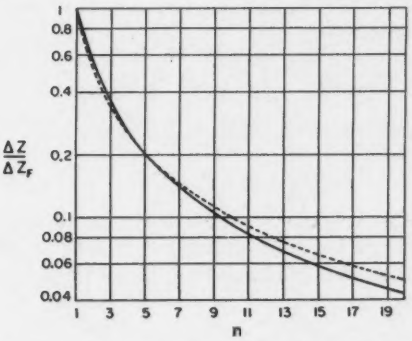

FIG. 3. The input impedance of the antenna as a function of the refractive index n. (——— calculated from the variational formulation; - - - - - - calculated from Monteath's approximate theory.)

derived from the work of Monteath and Surtees, whose approximate formula for the change of impedance ΔZ_M can be written in our notation as

$$I^2(0)\, \Delta Z_M = \frac{\eta_0}{n} \int\int (H_t)^2\, ds$$

where the exact value of H_t can only be determined by solving the appropriate integral equation. The above workers show that as a first approximation H_t can be identified with the magnetic field tangential to the ground that would exist there if the ground were perfectly conducting. The integration is to be extended over the whole surface of the earth outside the plane of the disk. Hence $H_t = 2H_\phi^i$ and,

$$I^2(0)\, \Delta Z_M = \frac{4\eta_0}{n} \int_0^{2\pi} \int_a^\infty [H_\phi^i(\rho)]^2\, \rho\, d\rho\, d\phi.$$

Writing H_ϕ in terms of U_1^i (Equation [2c]) and inserting the expression for U_1^i as given by [23] into the above integral, it is easily shown that for $k_1a \gg 1$,

$$[35] \qquad \Delta Z_M = \frac{\eta_0 \exp(2jk_1a)}{4\pi j(k_1a)n}\left[k_1\int_0^h K(z')\,dz'\right]^2.$$

It is seen that ΔZ_M is inversely proportional to n and the ratio $(\Delta Z_M/\Delta Z_F)$ plotted in Fig. 3 is equal to $(1/n)$; this result is in good agreement with calculations obtained from the variational method except for large n, when ΔZ_M begins to deviate considerably from the true value. It should be noted that when $n = 1$, there is exact agreement between Storer's formula [34] and the result [35] obtained from Monteath's theory.

5. SECOND VARIATIONAL FORMULATION

The variational formulation presented in this section will be developed only for the case $n = 1$, that is when the antenna and ground plate are in free space. First, an integral equation for the transverse magnetic field over the area of the disk (which is equivalent to the surface current) will be obtained.

Setting $n = 1$, $k_1 = k_2 = k$, and $\alpha_1 = \alpha_2 = \alpha$, then over the plane $z = 0$, Equation [10] becomes

$$U_1^i(\rho, 0) = \int_0^\infty J_1(\lambda\rho)\, F_1(\lambda)\,\frac{\lambda^2 d\lambda}{\alpha}, \qquad \rho > a.$$

A comparison with Equation [8*a*] leads to the result

$$[36] \qquad U_1^s(\rho, 0) = -\,U_1^i(\rho, 0), \qquad \rho > a.$$

This relation is in fact valid in all planar diffraction problems and results from the symmetry of the radiation about the $z = 0$ plane. A Fourier-Bessel transform of [8*a*], together with condition [36], yields the following expression for $F_1(\lambda)$:

$$[37] \quad \lambda F_1(\lambda)/\alpha = -\int_0^a J_1(\lambda\rho')\, U_1^s(\rho')\,\rho'\,d\rho' + \int_a^\infty J_1(\lambda\rho')\, U_1^i(\rho')\,\rho'\,d\rho', \quad z=0.$$

Furthermore, E_ρ must vanish over the surface of the ground plate so that [11] becomes

$$[38] \qquad 0 = \int_0^\infty J_1(\lambda\rho)\, F_1(\lambda)\,\lambda^2 d\lambda \qquad \rho < a.$$

On substitution of [37] into [38], the following integral equation is obtained for $U^s(\rho)$:

$$[39] \qquad \int_0^a G_0(\rho, \rho')\, U^s(\rho')\,\rho'\,d\rho' = \int_a^\infty G_0(\rho, \rho')\, U^i(\rho')\,\rho'\,d\rho'$$

(the subscripts "1" in U_1^s and U_1^i will be omitted henceforth).

The new Green's function $G_0(\rho, \rho')$ is defined as

$$[40] \qquad G_0(\rho, \rho') = \int_0^\infty J_1(\lambda\rho)\, J_1(\lambda\rho')\,\alpha\,\lambda d\lambda, \qquad \alpha = (\lambda^2 - k^2)^{\frac{1}{2}}.$$

It must now be pointed out that the integral defining $G_0(\rho, \rho')$ is not integrable and it diverges at the upper limit. The same difficulty exists in Levine and Schwinger's first paper (8) and on that account their work was criticized by

Copson. Bouwkamp (4), by a rather lengthy procedure, was able to show, however, that their whole theory can be developed free from any divergent integrals, and it is believed that similar objections to the present development can be likewise removed, although no attempt to do so will be made here.

The input impedance of the antenna is again as in [16] given by

$$[41] \qquad \Delta Z\, I(0) = -\lim_{\rho \to 0} \int_0^h E_z^s(\rho, z')\, K(z')\, dz',$$

and by a method similar to that given previously, E_z^s must be expressed again as a function of the unknown, which in this case is the value of $U^s(\rho)$ over the ground plate. As a result of some lengthy algebraic manipulation, it can be shown that

$$[42] \qquad \frac{jI^2(0)}{4\pi\omega\epsilon}\,\Delta Z = \int_0^\infty G_0(\rho, \rho')\, U^t(\rho')\, \rho'\, d\rho' \int_0^a U^s(\rho)\, \rho\, d\rho - \int_0^\infty G_0(\rho, \rho')\, U^t(\rho')\, \rho'\, d\rho' \int_a^\infty U^t(\rho)\, \rho\, d\rho.$$

Now multiply both sides of the integral equation [39] by $\rho U^s(\rho)$ and integrate from 0 to a; hence,

$$[43] \qquad \int_0^a \int_0^a G_0(\rho, \rho')\, U^s(\rho)\, U^s(\rho')\, \rho\, \rho'\, d\rho\, d\rho' = \int_0^a U^s(\rho)\, \rho\, d\rho \int_a^\infty G_0(\rho, \rho')\, U^t(\rho')\, \rho'\, d\rho'.$$

The right-hand side of [43] will now be denoted by R and rewritten as

$$R = \int_0^a U^s(\rho)\, \rho\, d\rho \int_0^\infty G_0(\rho, \rho')\, U^t(\rho')\, \rho'\, d\rho' - \int_0^a U^s(\rho)\, \rho\, d\rho \int_0^a G_0(\rho, \rho')\, U^t(\rho')\, \rho'\, d\rho'.$$

It follows from [39] and from the symmetry of $G_0(\rho, \rho')$ in ρ and ρ' that

$$\begin{aligned} R &= \int_0^a U^s(\rho)\, \rho\, d\rho \int_0^\infty G_0(\rho, \rho')\, U^t(\rho')\, \rho'\, d\rho' \\ &\quad - \int_a^\infty G_0(\rho, \rho')\, U^t(\rho')\, \rho'\, d\rho' \int_0^a U^t(\rho)\, \rho\, d\rho \\ &= \int_0^a U^s(\rho)\, \rho\, d\rho \int_0^\infty G_0(\rho, \rho')\, U^t(\rho')\, \rho'\, d\rho' \\ &\quad - \int_a^\infty G_0(\rho, \rho')\, U^t(\rho')\, \rho'\, d\rho' \int_0^\infty U^t(\rho)\, \rho\, d\rho \\ &\quad + \int_a^\infty G_0(\rho, \rho')\, U^t(\rho')\, \rho'\, d\rho' \int_a^\infty U^t(\rho)\, \rho\, d\rho \end{aligned}$$

and by comparison with [42] it is seen that

$$R = \frac{jI^2(0)}{4\pi\omega\epsilon}\,\Delta Z + \int_a^\infty \int_a^\infty G_0(\rho, \rho')\, U^t(\rho)\, U^t(\rho')\, \rho\, \rho'\, d\rho\, d\rho'.$$

The above double integral is independent of the unknown $U^s(\rho)$ and is only a function of the radiation characteristics of the antenna and of the dimensions of the ground plate: it will be taken as being proportional to a quantity Z_0 and defined specifically as

$$[44] \qquad \frac{jI^2(0)}{4\pi\omega\epsilon} Z_0 = \int_a^\infty \int_a^\infty G_0(\rho, \rho')\, U^i(\rho)\, U^i(\rho')\, \rho\, \rho'\, d\rho\, d\rho'.$$

Therefore R becomes

$$R = \frac{jI^2(0)}{4\pi\omega\epsilon} [\Delta Z + Z_0]$$

so that from [43] the following relation is obtained:

$$[45] \qquad \frac{jI^2(0)}{4\pi\omega\epsilon} [\Delta Z + Z_0] = \int_0^a \int_0^a G_0(\rho, \rho')\, U^s(\rho)\, U^s(\rho')\, \rho\, \rho'\, d\rho\, d\rho'.$$

On multiplying both sides of [45] by $[\Delta Z + Z_0]$ and using the relationship [43], it is found that

$$[46] \quad \frac{jI^2(0)}{4\pi\omega\epsilon} [\Delta Z + Z_0] = \frac{\left[\int_0^a U^s(\rho)\, \rho\, d\rho \int_a^\infty G_0(\rho, \rho')\, U^i(\rho')\, \rho'\, d\rho'\right]^2}{\int_0^a \int_0^a G_0(\rho, \rho')\, U^s(\rho)\, U^s(\rho')\, \rho\, \rho'\, d\rho\, d\rho'}.$$

ΔZ as given by [46] can be shown to be stationary with respect to small variations in $U^s(\rho)$ and $U^s(\rho')$ about their true value. Following Levine and Schwinger, a method of solving [46] will now be outlined.

A series expansion for the distribution of $U^s(\rho)$ over the plane of the disk is assumed to be of the form

$$[47] \qquad U^s(\rho) = \rho \sum_{n=1}^{\infty} a_n [1 - (\rho/a)^2]^{n-\frac{1}{2}}$$

where a_n are as yet unknown coefficients. The function [47] vanishes at the rim ($\rho = a$) as required by the edge conditions (3, 11) and it is zero at the center of the disk ($\rho = 0$). The latter is a consequence of the fact that

$$\lim_{\rho \to 0} H_\phi(\rho) = I(0)/2\pi\rho$$

and since in the limit $\rho \to 0$ the components H_ϕ^i and H_ϕ^r each contribute the amount $I(0)/4\pi\rho$, H_ϕ^s (and hence U^s) must vanish.

If the Green's function $G_0(\rho, \rho')$ and the series expansion [47] are substituted into the denominator of [46] a double sum is obtained whose individual terms are

$$D_{nm} = \int_0^\infty \alpha\, \lambda d\lambda \int_0^a J_1(\lambda\rho)[1 - (\rho/a)^2]^{n-\frac{1}{2}} \rho^2 d\rho \int_0^a J_1(\lambda\rho)[1 - (\rho/a)^2]^{m-\frac{1}{2}} \rho^2 d\rho.$$

The inner integrals can be evaluated with the aid of Sonine's identity (see Reference (9), p. 30) with the result that

$$D_{nm} = (k^2 a^5/2)(2/ka)^{n+m} \Gamma(n + \tfrac{1}{2}) \Gamma(m + \tfrac{1}{2}) \times \int_0^\infty J_{n+3/2}(kav)\, J_{m+3/2}(kav)\, v^{-(n+m)} (v^2 - 1)^{\frac{1}{2}}\, dv$$

where a new variable of integration $v = \lambda/k$ has been introduced.

Similarly the individual terms of the series appearing in the numerator of [46] are of the form

$$N_n = \int_0^\infty \alpha\, \lambda d\lambda \int_0^a J_1(\lambda\rho)[1 - (\rho/a)^2]^{n-\frac{1}{2}}\rho^2 d\rho \int_a^\infty J_1(\lambda\rho)\, U^t(\rho)\, \rho\, d\rho$$

$$= (ka^5/2)^{\frac{1}{2}}(2/ka)^n\Gamma(n + \tfrac{1}{2}) \times \int_0^\infty J_{n+3/2}(kav)\, v^{-n+\frac{1}{2}}(v^2 - 1)^{\frac{1}{2}}dv \int_{ka}^\infty J_1(uv)\, U^t(u/k)\, u\, du$$

with $u = k\rho$. On substituting the expressions for D_{nm} and N_n into Equation [46] it is found that the latter can be written in the form

$$[48a] \qquad \frac{jI^2(0)\, k}{4\pi\omega\epsilon}[\Delta Z + Z_0] = \left(\sum_{n=1}^\infty a_n d_n\right)^2 \Big/ \sum_{n=1}^\infty \sum_{m=1}^\infty a_n a_m c_{mn}$$

where d_n and c_{mn} are defined as

$$[48b] \quad d_n = (2/ka)^n\Gamma(n + \tfrac{1}{2}) \int_0^\infty J_{n+3/2}(kav)\, v^{-n+\frac{1}{2}}(v^2 - 1)^{\frac{1}{2}}dv \times \int_{ka}^\infty J_1(uv)\, U^t(u/k)\, u\, du,$$

$$[48c] \quad c_{mn} = (2/ka)^{n+m}\Gamma(n + \tfrac{1}{2})\, \Gamma(m + \tfrac{1}{2}) \times \int_0^\infty J_{n+3/2}(kav)\, J_{m+3/2}(kav)\, v^{-(n+m)}(v^2 - 1)^{\frac{1}{2}}dv,$$

and where Z_0, written explicitly, is

$$[48d] \qquad \frac{jI^2(0)\, k}{4\pi\omega\epsilon} Z_0 = \int_0^\infty (v^2 - 1)^{\frac{1}{2}} v dv \left[\int_{ka}^\infty J_1(uv)\, U^t(u/k)\, u du\right]^2.$$

The coefficients a_n are determined from the stationary property of ΔZ. Applying a small variation δa_n to the coefficients a_n, it then follows from [48a] that

$$[49] \qquad d_m \sum_{n=1}^\infty a_n\, d_n = \frac{jI^2(0)\, k}{4\pi\omega\epsilon}[\Delta Z + Z_0] \sum_{n=1}^\infty a_n c_{mn}, \qquad (m = 1, 2, \ldots).$$

We have however from [43] and [45] that

$$\frac{jI^2(0)}{4\pi\omega\epsilon}[\Delta Z + Z_0] = \int_0^a U^s(\rho)\, \rho\, d\rho \int_a^\infty G_0(\rho, \rho')\, U^t(\rho')\, \rho'\, d\rho'$$

and on substituting for $G_0(\rho, \rho')$ and $U^s(\rho)$ from [40] and [47] respectively, it follows that

$$[50] \qquad \frac{jI^2(0)}{4\pi\omega\epsilon}[\Delta Z + Z_0] = (ka^5/2)^{\frac{1}{2}} \sum_{n=1}^\infty a_n\, d_n.$$

Elimination of $(\Delta Z + Z_0)$ from [49] and [50] gives the following system of equations for the unknown coefficients a_n:

$$[51] \qquad \sum_{n=1}^\infty a_n\, c_{mn} = (2/k^3a^5)^{\frac{1}{2}}\, d_m, \qquad (m = 1, 2, \ldots).$$

An approximate solution of [51] is obtained by assuming $a_n = 0$ when $n > N$ and by solving only for the coefficients $a_1, a_2, \ldots, a_N$ from the first N equations of [51]. The impedance is then given approximately by

$$\frac{jI^2(0)}{4\pi\omega\epsilon}[\Delta Z + Z_0] \doteq (ka^5/2)^{\frac{1}{2}} \sum_{n=1}^{N} a_n d_n .$$

Levine and Schwinger have shown that by taking only two terms in their series for the coefficients, very accurate results could thus be obtained over a considerable frequency range.

No numerical calculations have as yet been made owing to some difficulty in evaluating the integrals that occur in [48*b*] and [48*d*]; it appears as if one must resort to numerical integration (the integral in [48*c*] can be evaluated in the same manner as was done in Levine and Schwinger's first paper).

APPENDIX

The solution of the following integral is required:

$$[A.1] \qquad k_1 B(a, b) = j\pi \int_0^\infty H_0^{(1)}(ay)\, H_0^{(1)}(by)\, dy$$

$$= j\pi \int_0^\infty J_0(ay)\, H_0^{(1)}(by)\, dy - \pi \int_0^\infty Y_0(ay)\, H_0^{(1)}(by)\, dy$$

for, say, $b > a$. Owing to the symmetry of the integral in a and b, an identical procedure to that given here applies when $b < a$; in the final result the roles of a and b must then be interchanged. Y_0 is a Neumann function of order zero, which for any order ν (zero, integral, or nonintegral) is defined in terms of Bessel functions by

$$[A.2] \qquad Y_\nu(z) = (\sin \nu\pi)^{-1}(\cos(\nu\pi)\, J_\nu(z) - J_{-\nu}(z)).$$

By applying the proper limiting procedure it is found from [A.2] that

$$Y_0(z) = \lim_{\nu \to 0} Y_\nu(z) = (2/\pi) \lim_{\nu \to 0} \frac{\partial}{\partial \nu}[J_\nu(z)]$$

and substituting this relation for Y_0 into [A.1] gives

$$[A.3] \qquad k_1 B(a, b) = j\pi \lim_{\nu \to 0} \int_0^\infty J_\nu(ay)\, H_0^{(1)}(by)\, dy$$

$$- 2 \lim_{\nu \to 0} \frac{\partial}{\partial \nu} \int_0^\infty J_\nu(ay)\, H_0^{(1)}(by)\, dy.$$

In [A.3] appears the integral

$$[A.4] \qquad I(a, b) = \int_0^\infty J_\nu(ay)\, H_0^{(1)}(by)\, dy$$

which must now be evaluated for an arbitrary value of ν.

Substituting the series expansion

$$J_\nu(z) = \sum_{r=0}^{\infty} \frac{(-1)^r (z/2)^{\nu+2r}}{r!\, \Gamma(\nu + r + 1)}$$

into [A.4] gives

$$[A.5] \qquad I(a,b) = \sum_{r=0}^{\infty} \frac{(-1)^r (a/2)^{\nu+2r}}{r!\,\Gamma(\nu+r+1)} \int_0^{\infty} y^{\nu+2r} H_0^{(1)}(by)\, dy.$$

Making use of the relation, (6),

$$\int_0^{\infty} t^{m-1} H_0^{(1)}(bt)\, dt = -(2j/\pi) \exp(j\pi m/2)\, 2^{m-2}\, a^{-m} (\Gamma(m/2))^2$$

it follows that

$$[A.6] \quad I(a,b) = (\pi b)^{-1} \sum_{r=0}^{\infty} \frac{(-1)^r \exp(j[\pi/2][\nu+2r])}{r!\,\Gamma(\nu+r+1)} \left(\frac{a}{b}\right)^{\nu+2r} [\Gamma(\tfrac{1}{2}\{\nu+2r+1\})]^2.$$

Substituting [A.6] into [A.3] leads to

$$[A.7] \quad k_1 B(a,b) = (j/b) \sum_{r=0}^{\infty} \frac{1}{(r!)^2} \left(\frac{a}{b}\right)^{2r} [\Gamma(r+\tfrac{1}{2})]^2$$

$$- (2/\pi b) \lim_{\nu \to 0} \frac{\partial}{\partial \nu} \sum_{r=0}^{\infty} \frac{1}{r!} \left(\frac{a}{b}\right)^{\nu+2r} \frac{\exp(j\pi\nu/2)}{\Gamma(\nu+r+1)} [\Gamma(\tfrac{1}{2}\{\nu+2r+1\})]^2.$$

On carrying out the differentiation with respect to ν, the imaginary part of [A.7] vanishes by cancellation of terms and one obtains the result that

$$k_1 B(a,b) = -(2/\pi b) \sum_{r=0}^{\infty} \frac{[\Gamma(r+\tfrac{1}{2})]^2}{(r!)^2} \left(\frac{a}{b}\right)^{2r} \left[\ln \frac{a}{b} + \psi(r+\tfrac{1}{2}) - \psi(r+1)\right]$$

where ψ is given by

$$\psi(z) = \frac{d \ln \Gamma(z)}{dz}.$$

In particular, if C denotes Euler's constant (0.5772 . .),

$$\psi(1) = -C,$$

$$\psi(n+1) = -C + 1 + 1/2 + 1/3 + \ldots + 1/n,$$

$$\psi(\tfrac{1}{2}) = -C - 2\ln 2,$$

$$\psi(\tfrac{1}{2} \pm n) = -C - 2\ln 2 + 2[1 + 1/3 + 1/5 + \ldots + 1/(2n-1)].$$

REFERENCES

1. Abbott, F. R. Proc. I.R.E. 40: 846. 1952.
2. Bardeen, J. Phys. Rev. 36: 1482. 1930.
3. Bouwkamp, C. J. Physica, 12: 467. 1946.
4. Bouwkamp, C. J. New York University, Mathematical Research Group, Research Report No. EM-50. 1953.
5. Brown, G. H., Lewis, R. F., and Epstein, J. Proc. I.R.E. 25: 753. 1937.
6. Gray, A., Mathews, G. B., and MacRobert, T. M. Treatise on Bessel functions. 1922. p. 66.
7. Leitner, A. and Spence, R. D. J. Appl. Phys. 21: 1001. 1950.
8. Levine, H. and Schwinger, J. Phys. Rev. 74: 958. 1948; 75: 1430. 1949.
9. Magnus, W. and Oberhettinger, F. Special functions of mathematical physics. Chelsea Pub. Co., New York. 1949. p. 2.
10. Meier, A. S. and Summers, W. P. Proc. I.R.E. 37: 609. 1949.
11. Meixner, J. Ann. Physik, (6) 6: 1. 1949.
12. Monteath, G. D. Proc. Inst. Elec. Engrs. (London), Pt. IV, 98: 23. 1951.
13. Norton, K. A. Proc. I.R.E. 24: 1367. 1936; 25: 1203. 1937.

14. SCHELKUNOFF, S. A. Advanced antenna theory. J. Wiley & Sons, Inc., New York. 1952. pp. 55, 56.
15. SOMMERFELD, A. Partial differential equations in physics. Academic Press Inc., New York. 1949. Chap. VI.
16. STORER, J. E. Harvard University, Cruft Laboratory Technical Report No. 119. 1950; J. Appl. Phys. 22: 1058. 1951.
17. STRATTON, J. A. Electromagnetic theory. McGraw-Hill Book Company, Inc., New York and London. 1941. p. 440.
18. SURTEES, W. J. University of Toronto, Department of Electrical Engineering. Report to the Defence Research Board under Grant DRB-67.

THE RADIOACTIVE ISOTOPES Al^{24}, P^{28}, Cl^{32} [1]

By S. W. Breckon,[2] A. Henrikson, W. M. Martin,[3] and J. S. Foster

ABSTRACT

The positron emitters P^{28} ($0.29 \pm .01$ sec.) and Cl^{32} ($0.32 \pm .01$ sec.) have been discovered in (p, n) reactions with thresholds at 15.4 ± 0.6 Mev. and 14.5 ± 0.6 Mev. respectively. Identification is realized through threshold and transition energies as well as through the complex γ-ray spectra identified in part with the known levels of the daughters Si^{28} and S^{32}.

The new nuclei represent an extension to the series $A = 4k$, $Z = 2k + 1$, whose initial members, B^8, N^{12}, Na^{20}, are delayed α-emitters, while the recently reported Al^{24} is known to emit delayed alphas or protons.

Under re-examination of Al^{24}, a half-life of $2.0 \pm .1$ sec. is obtained for γ-ray activity which identifies the stable daughter Mg^{24}.

The results are in substantial agreement with the recent work of Glass, Jensen, and Richardson. Delayed α-particles are not observed with the new isotopes.

INTRODUCTION

There exists a series of neutron-deficient radioactive isotopes characterized by $A = 4k$, $Z = 2k + 1$ (k an integer), in which delayed heavy-particle emission has been identified with each of the previously known members, B^8, N^{12}, Na^{20}, and Al^{24}. The first three of these, discovered by Alvarez (2), decay by positron emission of short half-life, and in each case at least one branch leads to an excited state of the daughter nucleus which in turn decays "instantaneously" by α-particle emission. The apparent lifetime of the α-emission is that of the respective parent, with which it is in equilibrium. Ann Birge (4) has observed heavy particles from Al^{24} in a similar type of decay, but it was not known whether this was an α-particle or proton emission since either kind is energetically possible in this case.

Al^{24}, produced by proton bombardment of a magnesium target, was selected as the most convenient of these isotopes to study with the pneumatic target-extractor (14) of the McGill University proton synchrocyclotron. The investigation was undertaken to observe with a scintillation spectrometer possible γ-ray transitions from excited states of the stable daughter Mg^{24}, and by the use of similar techniques to search for additional members of this radioactive series.

Following the above procedure, two new members of the series, P^{28} and Cl^{32}, have been discovered with short half-lives following proton bombardment of silicon and sulphur respectively, but varied efforts to detect new α-emissions have been unsuccessful. Gamma-rays observed in the new activities, as well as for Al^{24}, confirm the assignments.

Meanwhile, Glass, Jensen, and Richardson (9) have published results many of which are in substantial agreement with those reported here.

[1] *Manuscript received September 15, 1953.*
Contribution from the Radiation Laboratory, McGill University, Montreal, Quebec.
The method and principal results of this work including corrected half-lives for P^{28} and Cl^{32} were presented as paper No. 52, Section III, to the Royal Society of Canada at the June meeting, 1953.

[2] *Now at Memorial University of Newfoundland, St. John's, Newfoundland.*
[3] *Present address: Queen's University, Kingston, Ontario.*

THE EXPERIMENTAL METHOD

1. *Equipment*

The operation of those parts of the equipment near the cyclotron may be described briefly as follows: when short half-life activities are being observed, the control circuits of the cyclotron are interlocked with those of the pneumatic extractor. After a brief period of bombardment, the targets are shot back to a position of minimum magnetic field near the cyclotron, where suitably-shielded scintillation counters detect the radiations of interest. The pulses are transmitted to the main laboratory where they are amplified, shaped, and recorded. Recording is accomplished with the use of scalers, a counting-rate meter, and by photographing a cathode-ray tube display for pulse-height analysis.

The basic mechanical and electronic apparatus has been described in a previous paper (14). Since then the principal alterations and additions which have been carried out include

(*a*) provision for the simultaneous use of two counters with the extractor unit;

(*b*) a duplicate amplifying and pulse-shaping system for use with the second counter;

(*c*) a single-sliding-channel pulse-height analyzer which can accept pulses at the rate of several thousand a second;

(*d*) an electronically-controlled sweep circuit for the oscilloscope display of the counting-rate meter output;

(*e*) a pulse-shaping and pulse-height display system which includes the following units: a pulse shaper adapted from a design by Watkins (15), a stepped-attenuator with a pulse-height limiter, a Los Alamos Model 1000 amplifier (8), and a Tektronix cathode-ray oscilloscope, type 513 D with a 5XP11 tube.

A second counter is sometimes needed to monitor the radioactivity from various runs if different absorbers are being used in conjunction with the first counter. In general, one counter was used for γ-ray detection, the other for β or α-particle detection.

The single-channel analyzer aided in the early setting up and calibration of the γ-ray scintillation spectrometer.

Owing to the short-period nature of the radiations under study, and the need for accumulating a sufficient number of pulses to give good statistics in the pulse-height spectrum, the display and recording system has been arranged so as to be capable of handling rates up to approximately ten thousand pulses per second.

Pulses from the first amplifier are lengthened in duration at the peak amplitudes, and are then passed through a second amplifier which drives the Y-plates of the Tektronix oscilloscope. An individual pulse thus shows over much of its duration as a horizontal trace, its distance from the undeflected position being a measure of the pulse-height. The attenuator is used to expand the pulse-height scale, the limiter ensuring that the second amplifier is not

overloaded by the larger pulses. It is thus possible to examine the lower energy portion of a spectrum.

The pulses displayed on the cathode-ray tube are photographed and an energy analysis of the spectrum is made directly from prints obtained from the negative.

2. *Gamma-ray Scintillation Crystal Spectrometer*

The single-crystal scintillation spectrometer for the detection of γ-rays was constructed using a polished NaI (Tl) crystal 1 in. in diameter and 1 in. long. This crystal was held in an aluminum container by aluminum foil which not only smoothly covered the back end and side of the crystal, but which also served as a packing. The remaining space in the container was filled with mineral oil, and the whole assembly held against the end of an R.C.A. 5819 photomultiplier, with an O-ring providing the seal.

This system gave an energy resolution of about 11% with the photopeak of the 0.661 Mev. γ-ray from Cs^{137},* and remained essentially the same over a period of six months, the crystal being left undisturbed. The resolution is defined as the full width at half the peak counting rate, expressed as a percentage of pulse height at the peak. It was observed that the resolution varied as $1/\sqrt{E}$ in the energy range investigated (33 kev. to 3.41 Mev.).

Each amplifying and pulse-shaping circuit was checked for pulse-height linearity over its useful range by means of a pulse generator. A similar check was made with the electronic units operating together. The spectrometer as a whole was shown to be linear by calibration with γ-rays of known energies, from Cs^{137}, ThC″, a Po–Be source, and Co^{60}. It was found by experiment that the magnetic field of the cyclotron did not affect the linearity of the shielded counters.

In the course of the above calibration experiments, runs were taken with the single-channel analyzer in order to compare the relative intensities of the peaks making up a pulse-height spectrum. Here, "relative intensities" refers to the relative numbers of pulses of which the peaks are comprised. These peaks are present as a result of the different processes in which γ-rays interact with the scintillation crystal.** For a given NaI (Tl) crystal, the number of peaks per γ-ray arising from these processes depends principally upon the energy of the γ-ray, and to a lesser extent upon the energy resolution of the spectrometer.

Peaks from the photoelectric effect give the full energy, E_0, of the γ-ray, since the low energy secondary radiations are commonly absorbed in the crystal. Pair production gives rise to a pair peak, P_1, in processes from which both quanta of the annihilation leave the crystal (a peak, lying 1.02 Mev. lower than the photopeak), and to a less intense second peak when the energy of one of the quanta is absorbed completely in the crystal. The separation of these peaks is 0.51 Mev. In general, this second peak was not resolved

* *The Cs^{137} was very kindly loaned by Atomic Energy of Canada, Limited, Chalk River, Ontario.*

** *For an account of the contributions made to the pulse-height spectrum by these interactions, see, for example, Casson (6).*

from the peak of the Compton distribution. This composite peak has been designated P_2. In the above remarks, it is assumed that both electrons of the pair are stopped within the crystal.

At higher γ-ray energies, the P_1 peak predominates because of the increasing cross section for pair production relative to the photoelectric and Compton cross sections. Also, the peak giving the full energy, E_0, of the γ-ray, receives an increasing contribution from pair-production events which result in complete absorption of both electrons and quanta in the crystal.

In the bombardment of Mg, Si, or S at the energies used in this experiment, the incidental production of undesirable positron activities is unavoidable. To prevent these positrons as well as high energy positrons from Al^{24}, P^{28}, or Cl^{32} from entering the NaI (Tl) crystal, an absorber was placed between the crystal and the source position. This absorber, together with the crystal container, was sufficiently thick to stop electrons of energy up to 11.5 Mev.

A calibration of the gamma-spectrometer was carried out after each series of runs under conditions identical with those of the experiments.

3. *Analysis of the Pulse-height Spectra*

As a result of the previously mentioned limitations on the counting rate, it becomes desirable, in photographing the pulse-height display on the cathode-ray tube, to superimpose a number of similar exposures on the same photographic frame. This is done when necessary to ensure good statistical representation in the pulse-height spectrum.

In order to separate the record of the γ-rays of special interest from that due to the longer periods in the background, the following procedure was first adopted. A succession of short, timed exposures from separate bombardments were superimposed on the same frame. Then a zero-deflection trace was recorded as the reference line. Following this, the background was recorded in the succeeding run by an exposure on a separate frame for the same total time.

Fig. 1 shows a first frame from Al^{24}.

In a second method, with the camera aperture opened up, short exposures of two or more seconds each were taken in immediate sequence on separate frames and without further bombardment. These reveal the decay of the short half-life spectrum, since the later members of the sequence show only peaks due to longer-lived activities. Fig. 5*b*, which shows the spectrum from P^{28}, is the first of such a sequence.

In either method, the decay of the activity was also observable separately, on a cathode-ray tube presentation of the counting-rate meter output from which the half-lives were obtained. Fig. 4 shows the decay of Al^{24}, P^{28}, and Cl^{32} respectively.

The above procedures were repeated on different gain (attenuation) settings for examination of the lower energy parts of a spectrum. Not only were various camera apertures required to obtain a suitable negative, but a series of varied printing exposures were also required to render different parts of the spectrum suitable for pulse-height analysis.

A representative calibration spectrum from ThC″ may be seen in Fig. 2. The upper three peaks are the P_1, P_2, and photo of the 2.615 Mev. (10) γ-ray.

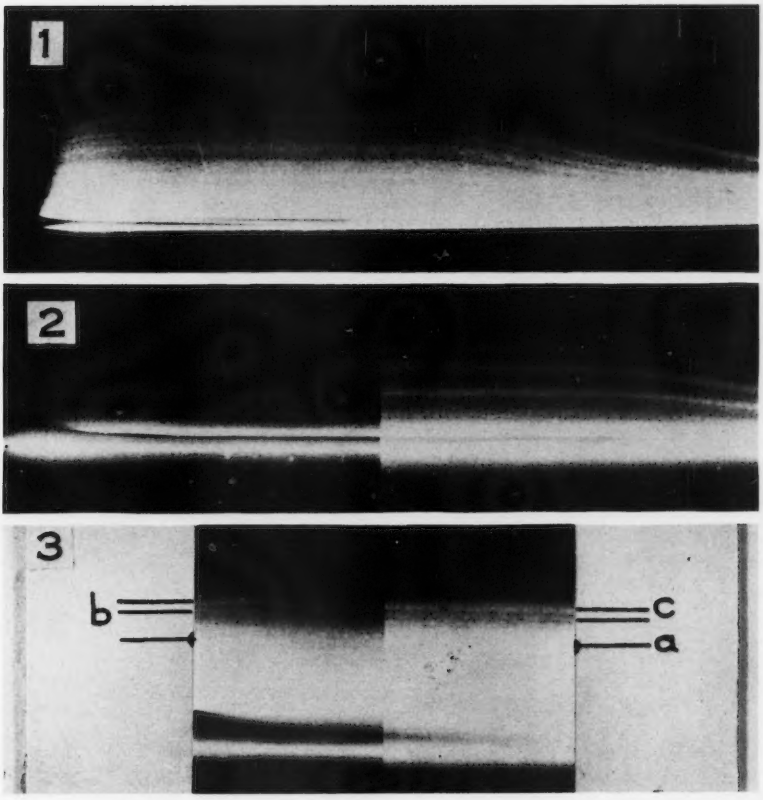

FIG. 1. A photograph of the pulse-height spectrum of the γ-rays from Al^{24}.

FIG. 2. A photograph of the pulse-height spectrum of the γ-rays from ThC''. The upper three peaks are the P_1, P_2, and photo of the 2.615 Mev. γ-ray. Two exposure times have been used in producing this print from the negative.

FIG. 3. A photograph of the low energy pulse-height spectrum of the γ-rays from P^{28}. Only part of the full pulse length is shown.

PLATE II

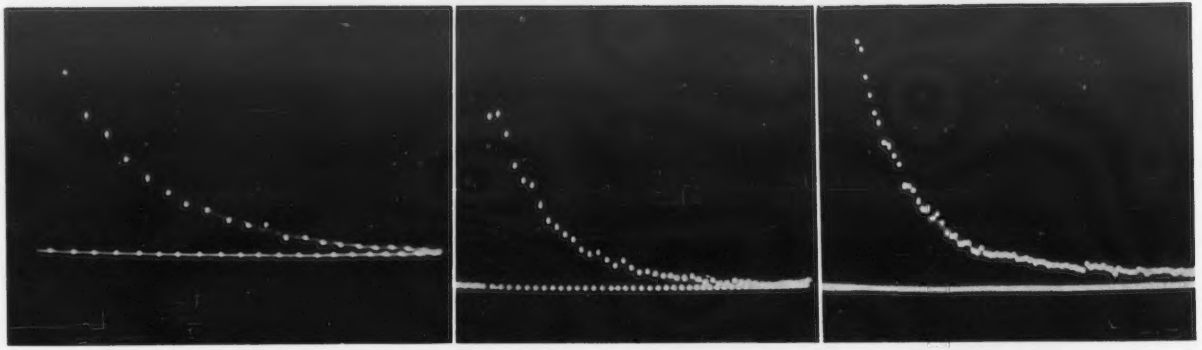

FIG. 4. Photographs of the decay of Al^{24}, P^{28}, and Cl^{32} (timing spots 2 per sec., 20 per sec., and 20 per sec. respectively).

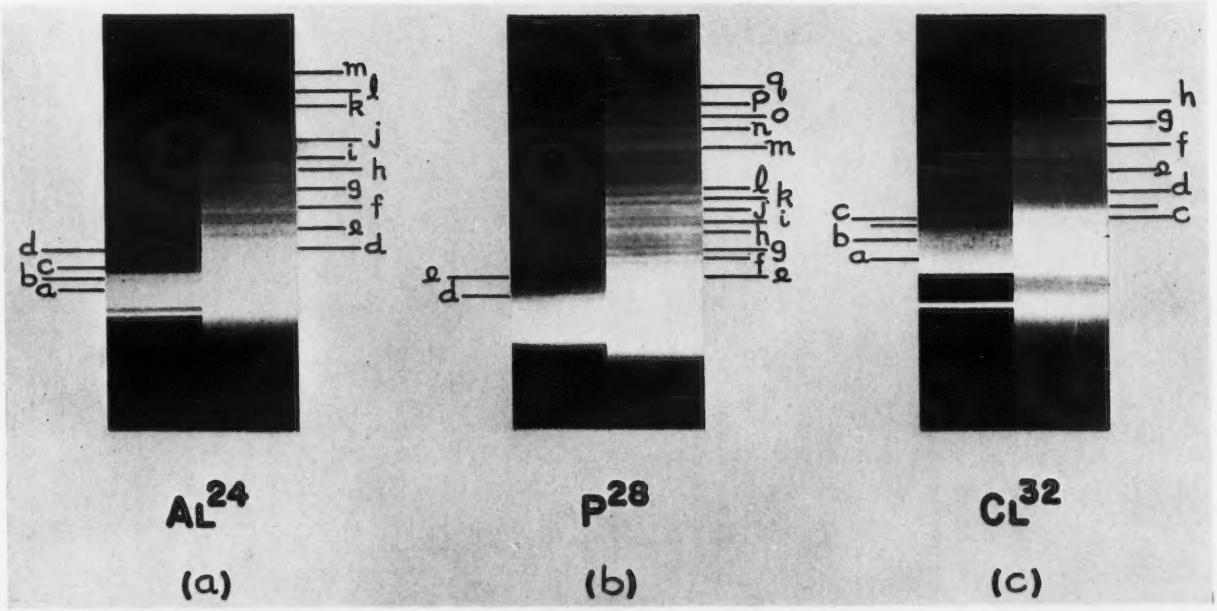

FIG. 5. Photographs of the pulse-height spectra of the γ-rays from Al^{24}, P^{28}, and Cl^{32}, respectively. Only part of the full pulse length is shown in each case. Two exposure times have been used in producing these prints from the negatives.

In the new spectra, if a peak was visible on several of the records, at the same location, it was accepted as 'genuine', that is, not due to statistical fluctuations. The energies of the peaks were determined by scaling the deflection distance directly from the photographic prints. An estimated error was placed on an individual measurement of the peak position. These were combined for all similar spectra analyzed, the resulting errors being used to obtain an estimated probable error in energy from the calibration graph.

Owing to the nature of P_2 peaks, the pulse amplitude at the peak does not vary linearly with γ-ray energy (due to the Compton component), and an energy determination made therefrom is not as certain as in the case of a P_1 or photopeak. For this reason, only P_1 and photopeaks were used for energy determinations.

4. *Targets*

Initially, magnesium, silicon, and sulphur targets were prepared from Matthey magnesium rod, fused quartz, and commercial grade sulphur, respectively.

Later, for additional γ-ray spectra, half-life and threshold determinations, and β-particle experiments, finely divided magnesium, silicon, and sulphur were enclosed in cobalt tubes of 1/16th in. diameter which were flattened to 1/32nd in. The cobalt foil used in constructing the tubes was 0.0014 in. thick, and in separate runs with the cobalt alone showed no short-period activity which could interfere with those being studied. Furthermore, with the short bombardments used, little activity was obtained from the foil itself. With the exception of the sulphur in one target with which only part of the work was done, the materials were of Matthey 'H.S.' Brand.

In the search for α-particles, targets of magnesium and sulphur were evaporated separately onto cobalt foils. Silicon targets were prepared by depositing a thin layer of Dow Corning silicone high vacuum grease or DC 200 fluid onto such a foil.

With the exception of runs for the determination of thresholds, all experiments were carried out at proton energies less than 20 Mev.

5. *Thresholds*

The relative yield as a function of the nominal energy of the proton beam was determined for Al^{24}, P^{28}, and Cl^{32} in much the same manner as described for previous experiments (14). The beam current remained sensibly constant throughout a determination, and bombardment periods were kept identical. Commencing at energies considerably above the threshold, several runs were taken at each of a number of selected cyclotron radii, which gave nominal proton energies covering the energy range in steps to below the threshold. The thresholds as determined from the curves of relative yield versus nominal proton energy, Fig. 6, were corrected for the proton energy loss in the cobalt foil enclosing the target material. The thresholds of the new activities were then determined relative to that for Al^{24} which has been measured by Birge (4) using the Berkeley proton linear accelerator.

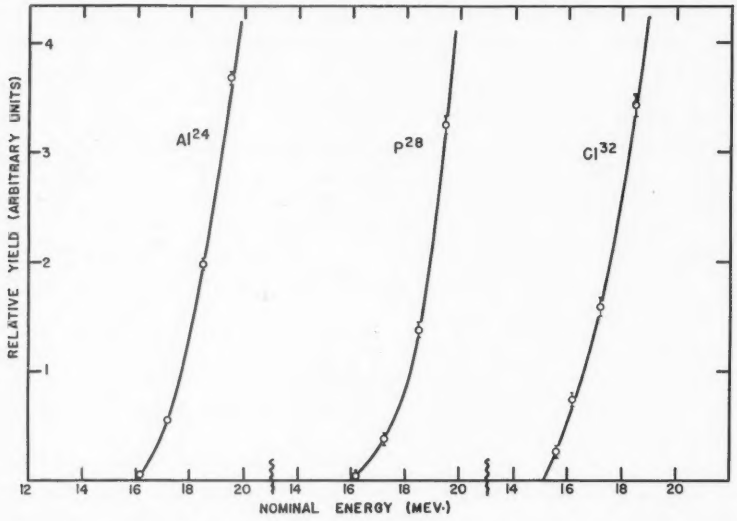

FIG. 6. Relative yield as a function of proton energy.

6. *Alpha-particle Experiments*

In preliminary experiments, an attempt was first made to detect the heavy particles from Al^{24} (4). Ilford D1 and C2 nuclear plates (emulsion 50 μ thick) were held in the normal counting position and repeatedly exposed to the radioactivity from Al^{24}. It was found, however, that background radiations were too intense for a practical result to be obtained. These were apparently due, for the most part, to hydrogen atoms of energies up to about 2 Mev. which originated in the main tank of the cyclotron.

Attempts were then made to detect heavy particles using scintillation counters. One of these had a $\frac{1}{2}$ mm. thick NaI (Tl) crystal, the other a ZnS (Ag) screen. Calibration was realized with Po^{210} α-particles which were reduced in energy by aluminum absorbers. Results obtained with the NaI (Tl) crystal were inconclusive and so it was discarded.

7. *Beta-particle Detection*

A trans-stilbene crystal scintillation counter was used for the detection of β-particles. The crystal was in the form of a truncated cone, 1 cm. in diameter at the small end, $2\frac{1}{2}$ cm. at the large end, and 4 cm. long. The counter was so held that the target source resided at the apex of the truncated cone. With an RCA 5819 photomultiplier, an energy resolution of 15% was obtained on the 625 kev. conversion electrons from a Cs^{137} source. Originally this counter was designed for high energy β-particle measurements with isotopes which had little γ-ray activity. As such, it was not ideally suited to the present work, the crystal efficiency for γ-rays being higher than desired.

The object of the experiments with the stilbene counter was to observe

whether or not the placing of aluminum absorbers of increasing thickness between the source and the counter would reduce the activity by amounts indicative of the presence of β-particles. At the same time use could be made of a variable pulse-height discriminator in the electronic circuitry to determine the change in the integral pulse-height distribution with an increase in absorber thickness. Simultaneously the NaI (Tl) counter monitored the short-period γ-ray activity for normalization purposes.

To reduce interference from β-particles of other activities with half-lives of the order of several seconds, it was desirable to have an 'initial' absorber between the stilbene crystal and the source. Threshold and γ-ray transition energies of the new activities had already indicated the probable existence of high energy β-particles, many of which would penetrate through such absorbers. In the first series of experiments, therefore, comparison was made between the activities observed with absorbers which would stop 5 Mev. and 10 Mev. β-particles respectively. In the second series comparison was made between absorbers which would stop 3, 5, and 10 Mev. β-particles. Owing to time and space limitations of the experiment it was not feasible either to increase the number of absorbers, or to increase the thickness beyond that of the 10 Mev. absorber.

EXPERIMENTAL RESULTS

1. *The New Isotopes, P^{28} and Cl^{32}*

A summary of the isotope data obtained for the new isotopes, as well as for Al^{24}, is given in Table I. Each half-life determination is the mean of 10 or

TABLE I

ISOTOPE DATA

Isotope	Al^{24}	P^{28}	Cl^{32}
Half-life (sec.)	2.0 ± 0.1	$0.29 \pm .01$	$0.32 \pm .01$
Type of decay	β^+	β^+	β^+
Produced in reaction	(p, n)	(p, n)	(p, n)
Threshold (Mev.)	Birge value 15.4 ± 0.3	15.4 ± 0.6	14.5 ± 0.6
Calculated atomic mass (a.m.u.)	—	$28.0009 \pm .0008$	$31.9964 \pm .0008$

more analyzed runs with the counting-rate meter, the error being the standard deviation from the mean. Evidence shows that β-particles are present in the decays. That these are positrons, however, must be inferred from the neutron-deficient nature of the isotopes, since clear observation of annihilation radiation is prevented by heavy background activity. Furthermore, the layout of the target-extractor equipment precluded the use of any magnetic method for identification of the particles.

The thresholds for the production of P^{28} and Cl^{32} have been determined relative to Birge's value of $15.4 \pm .3$ Mev. for Al^{24} (4). It is interesting to note

here that on the basis of the nominal energy of protons in the McGill cyclotron, this latter threshold was also measured as 15.4 Mev. The atomic masses have been calculated using the masses of Si^{28} and S^{32} given by Li (12).

The assignment of the new activities to P^{28} and Cl^{32} has been made on the basis of threshold and transition energies, and on the identification of certain observed γ-ray transitions with the level structures reported for the daughters Si^{28} and S^{32} respectively. These transitions are discussed in subsequent sections. Since at least 8 Mev. transition energy is associated with P^{28} decay, reactions other than (p, n) which would produce new isotopes with the observed threshold are not possible. Similar arguments apply to the case of Cl^{32} which has a transition energy of at least 4.8 Mev. Further evidence that these activities are produced from the low mass isotopes of the target elements is supplied by the failure to obtain them on bombardment of phosphorus and chlorine respectively, with protons up to 60 Mev.

2. *The Gamma-ray Spectrum of Al^{24}*

Representative pulse-height-spectra from the γ-rays of Al^{24} are given in Figs. 1 and 5*a* which have different pulse-height scale factors. Over 30 spectra were examined to obtain the results of Table II which summarizes the observed peaks and the probable γ-rays which give rise to them.

TABLE II

GAMMA-RAYS OBSERVED WITH THE DECAY OF Al^{24}

P_1: pair peak with escape of both annihilation quanta, at $E_0 - 2mc^2$.
P_2: unresolved pair peak with escape of one annihilation quantum, and the Compton peak, at approximately $E_0 - mc^2$.
E_0: photopeak plus other processes adding up to the full energy E_0 of the γ-ray.

Peak identification (see Fig. 5*a*)	Observed peak location (Mev.)	Probable peak assignment	Energy of associated γ-ray (Mev.)
a	0.98 ± .04	Compton	1.38
b	1.38 ± .04	Photo	1.38 ± .04
c	1.70 ± .06	P_1	2.72 ± .06
d	2.24 ± .07	P_2	2.70
e	2.68 ± .09	Photo	2.68 ± .09
f	3.19 ± .12	P_1	4.21 ± .12
g	3.69 ± .13	P_2	4.21
h	4.35 ± .14	P_1	5.37 ± .14
i	4.64 ± .18	P_1	5.66 ± .18
j	5.04 ± .22	P_2	5.37
k	6.01 ± .24	P_1	7.03 ± .24
l	6.60 ± .25	P_2	7.03
m	7.00 ± .27	E_0	7.00 ± .27

All the photographs and tables have, in fact, been suitably arranged for convenient examination of the main features leading to estimates of γ-ray energies from each isotope. The reader may wish to inspect these features and conclusions before proceeding with the following paragraphs which deal with particulars less evident in a preliminary examination.

It will be noted that peaks* '*a*' and '*b*' appear to be of greater intensity (as

* *Such 'peaks' might be called 'lines' in this type of recording, but since the spectrometer has been described already in Experimental Method (Sect. 2), with reference to a single-channel analyzer where use of the term 'peak' is appropriate, we have retained the term throughout this article.*

defined in Experimental Method, Sect. 2) than any of the other labelled peaks. Taking into consideration γ-ray absorption in the aluminum, and the crystal efficiencies for γ-ray detection, it seems probable that there are more γ-rays of 1.38 Mev. than of any other single energy. Peak '*a*' stands out clearly in the spectrum when the pulse-height scale is expanded.

The estimated relative intensities of peaks '*c*' and '*e*' compare well with those of the P_1 and photopeak of a γ-ray of about 2.7 Mev., similar to the 2.615 Mev. γ-ray of the ThC'' in Fig. 2. It seems unlikely that there is any photopeak contribution to '*c*' from a 1.70 Mev. γ-ray, although evidence for a level in Mg^{24} at approximately this energy has been reported (13). Peak '*f*' stands out more clearly on most photographs than in this reproduction. The peak between '*g*' and '*h*' is spurious and does not show up in other spectra. Peak '*i*' is weak, and '*m*' is barely discernible except on the original negatives. The spectrum was not examined below an energy of about 800 kev.

The peaks of the spectrum of background radiations were of low energy, and in the examined region of the spectrum of Al^{24} also of low relative intensity.

3. *The Gamma-ray Spectrum of P^{28}*

The pulse-height spectrum from the γ-rays of P^{28}, shown in Fig. 5*b*, is the first of a sequence of exposures (see Experimental Method, Sect. 3). This is reproduced in preference to a multiple exposure photograph as it exhibits more clearly the peaks in the upper part of the spectrum, even though the statistics are not so good. Peaks '*k*' and '*l*', however, appear here with more than average relative intensities.

The results are summarized in Table III. In order to show peaks '*a*', '*b*', and

TABLE III

GAMMA-RAYS OBSERVED WITH THE DECAY OF P^{28}

P_1: pair peak with escape of both annihilation quanta, at $E_0 - 2mc^2$.
P_2: unresolved pair peak with escape of one annihilation quantum, and the Compton peak, at approximately $E_0 - mc^2$.

Peak identification (see Fig. 5*b* and Fig. 3)	Observed peak location (Mev.)	Probable peak assignment	Energy of associated γ-ray (Mev.)
a	1.42 ± .08	Compton	1.78
b	1.66 ± .06	P_1	2.68 ± .06
c	1.78 ± .04	Photo	1.78 ± .04
d	2.22 ± .07	P_2	2.66
e	2.66 ± .10	Photo	2.66 ± .10
		P_2	3.01
f	3.01 ± .07	Photo	3.01 ± .07
g	3.24 ± .12	[P_1]	4.26 ± .12
h	3.61 ± .10	P_1	4.63 ± .10
i	3.87 ± .09	P_1	4.89 ± .09
j	4.14 ± .12	P_2	4.63
		P_1	5.16 ± .12
k	4.44 ± .10	P_1	5.46 ± .10
		P_2	4.89
l	4.64 ± .10	Photo	4.64 ± .10
		P_2	5.16
m	5.63 ± .11	P_1	6.65 ± .11
n	6.06 ± .12	P_1	7.08 ± .12
o	6.42 ± .14	P_1	7.44 ± .14
p	6.71 ± .14	P_1	7.73 ± .14
q	7.10 ± .21	P_1	8.12 ± .21

'*c*', a multiple exposure photograph is reproduced in Fig. 3. A peak due to background radioactivity also appears at the location '*b*', but the evidence points to the existence of a short half-life component. For this reason the peak is included with the main group in Table III. No P_1 peak is recorded for the 3.01 Mev. γ-ray since it is difficult to resolve peaks in the region of '*d*'. However the spectrum above '*f*' is not readily interpreted in a manner which would make '*f*' a P_1 peak for a 4.03 Mev. γ-ray. Therefore it is probable that '*f*' is a photopeak as noted in Table III.

There appears to be a small peak between '*g*' and '*h*' in Fig. 5*b*, but evidence from other photographs indicates that it is probably spurious. Peak '*g*' is weak and the assignment as a P_1 uncertain. Peaks '*h*' and '*j*' are the two most prominent peaks in this region. Peak '*j*' is too intense relative to '*k*' to be solely a P_2 for a 4.63 Mev. γ-ray, and probably has a contribution from a P_1 peak. Peak '*k*' also appears to be too intense relative to '*i*' to be only a P_2 peak for a 4.89 Mev. γ-ray. In the upper part of the spectrum both '*m*' and '*n*' are P_1 peaks, since '*n*' is too intense relative to '*m*' and too near in energy to be a P_2 peak for the 6.65 Mev. γ-ray. The peaks above '*n*' are weak with '*o*' and '*p*' difficult to resolve, and the evidence for '*q*' obtained from only two photographs. A recent review of the experimental data has brought to light a possibility that these peaks may be in a nonlinear region of the spectrometer. Since the errors given are estimated on the basis of linearity, they may consequently be optimistic.

The spectrum below '*a*' is difficult to interpret. This is also the case with the spectrum of the background radiations, where, however, narrow peaks at $1.43 \pm .04$ and $1.28 \pm .04$ Mev. are evident. Apart from the above-mentioned peaks, background γ-rays of longer half-life introduce no complicating factors of appreciable magnitude in the higher energy regions.

4. *The Gamma-ray Spectrum of* Cl^{32}

A representative multiple-exposure photograph of the pulse-height spectrum of the γ-rays of Cl^{32} is reproduced in Fig. 5*c*. Results of energy measurements

TABLE IV

GAMMA-RAYS OBSERVED WITH THE DECAY OF Cl^{32}

P_1: pair peak with escape of both annihilation quanta, at $E_0 - 2mc^2$.
P_2: unresolved pair peak with escape of one annihilation quantum, and the Compton peak, at approximately $E_0 - mc^2$.

Peak identification (see Fig. 5*c*)	Observed peak location (Mev.)	Probable peak assignment	Energy of associated γ-ray (Mev.)
a	$1.26 \pm .04$	P_1	$2.28 \pm .04$
b	$1.83 \pm .08$	P_2	2.25
c	$2.23 \pm .05$	Photo	$2.23 \pm .05$
d	$2.77 \pm .08$	[P_1]	$3.79 \pm .08$
e	$3.31 \pm .09$	P_1	$4.33 \pm .09$
f	$3.80 \pm .08$	P_1	$4.82 \pm .08$
		P_2	4.33
g	$4.35 \pm .12$	P_2	4.82
h	$4.82 \pm .15$	Photo	$4.82 \pm .15$

of the peaks are given in Table IV. The prominent high energy peak '*f*', due principally to P_1, appears to be rather broad. This is probably due to a P_2 contribution from the 4.33 Mev. γ-ray. Peak '*e*' seems to be too intense relative to '*d*' to be only a P_2 peak for a possible 3.79 Mev. γ-ray.

It will be noted that two peaks which lie between '*b*' and '*c*', and '*c*' and '*d*', respectively, of Fig. 5*c*, are not included in the table. Additional experimental evidence obtained since this work was first reported (5) shows that these two peaks are not associated with the decay of Cl^{32}. Although photographic exposures of the spectrum of background radioactivity, taken in the normal manner, do not reveal their presence, a sequence of exposures shows peaks of similar energies remaining after the decay of the 0.32 sec. activity. It is concluded, therefore, that they have half-lifes of the order of several seconds. Their assignment as photopeaks gives γ-ray energies of 2.08 ± .05 Mev. and 2.44 ± .07 Mev. respectively. Furthermore, there is some doubt not only about the assignment of peak '*d*' as a P_1, but also about the assignment to Cl^{32}, since a weak peak is observed in the background at a location of 2.63 ± 0.09 Mev.

A peak of lower intensity than '*a*' also remains in the background spectrum at 1.28 ± .06 Mev. The other peaks in the spectrum of background radiations are weak and difficult to assign. However they do not interfere to any appreciable extent with observations on the main spectrum.

Spectrum analysis was not attempted below a peak energy of about 1 Mev.

5. *Search for Alpha-particles*

In the search for α-particles with the ZnS (Ag) screen the discriminator bias was set at a value corresponding roughly to $\frac{3}{4}$ Mev. in energy so that any α-particle with energy greater than this would be detected. Heavy particles were detected following bombardment of magnesium, thus verifying the results of Birge (4). The experiment indicated the proportion of heavy particles from magnesium to be about 1 particle for about 300 γ-rays of energy greater than 1 Mev. This figure is obtained by correcting the observed counts for the different solid angles of the two counters, and correcting for the efficiencies of the ZnS screen and NaI crystal. No correction to the gamma count has been applied for bremsstrahlung radiation that may be present in unknown amount.

No α-particles were observed from targets of silicon or sulphur, indicating that if any are present the energy is less than $\frac{3}{4}$ Mev. or the branching is less than 1 alpha for 1000 gammas in the case of silicon and less than 1 alpha for 2000 gammas in the case of sulphur.

6. *Detection of Beta-particles*

In analyzing the results of the β-particle experiments it was assumed (i) that the percentage of γ-ray counts due to scattered radiation was constant in each counter and independent of the particular absorbers used with the stilbene; (ii) that changes in the total γ-ray count above 1 Mev., due to variation in the bremsstrahlung with the different absorbers used, were negligible. It is likely that use of the second assumption will tend to lessen any experimental evidence for β-particles rather than to strengthen it.

If, in connection with the β-counter, we now define the transmission of an absorber as

$$ {}_{E}T_{A} = \frac{\text{Number of pulses above pulse-height } E\text{, using absorber } A}{\text{Number of pulses above pulse-height } E\text{, with no absorber}} $$

where the absorber will stop completely β-particles of energy A, and if

$$ {}_{E}R_{A,B} = \left(\frac{{}_{E}T_{A}}{{}_{E}T_{B}}\right)_{\text{measured}} \div \left(\frac{{}_{E}T_{A}}{{}_{E}T_{B}}\right)_{\text{calculated for } \gamma\text{-rays}} $$

then values of ${}_{E}R_{A,B}$ greater than unity will indicate that γ-rays can account for only a part of the radiation detected using the lighter absorber. Table V

TABLE V

TRANSMISSION OF ABSORBERS FOR γ-RAYS RECORDED BY β-COUNTER

$$ {}_{E}T_{A} = \frac{\text{Number of pulses above pulse-height } E\text{, using absorber } A}{\text{Number of pulses above pulse-height } E\text{, with no absorber}} $$

$$ {}_{E}R_{A,B} = \left(\frac{{}_{E}T_{A}}{{}_{E}T_{B}}\right)_{\text{measured}} \div \left(\frac{{}_{E}T_{A}}{{}_{E}T_{B}}\right)_{\text{calculated for } \gamma\text{-rays}} $$

Bias level		${}_{E}T_{3}/{}_{E}T_{5}$		${}_{E}R_{3,5}$	${}_{E}T_{5}/{}_{E}T_{10}$		${}_{E}R_{5,10}$
E, Mev.		Calc.	Measured		Calc.	Measured	
Al^{24}	1	1.07	1.19 ± .02	1.11	1.19	1.13 ± .02	0.95
	2	1.05	1.19 ± .02	1.13	1.12	1.11 ± .03	0.99
	3	1.04	1.20 ± .04	1.15	1.10	1.03 ± .03	0.94
	4	1.03	1.19 ± .04	1.15	1.09	1.04 ± .04	0.95
P^{28}	1	1.07	1.97 ± .09	1.84	1.19	2.57 ± .11	2.16
	2	1.05	2.20 ± .24	2.10	1.12	4.80 ± .34	4.28
	3	1.04	2.18 ± .19	2.10	1.10	6.17 ± .53	5.60
	4	1.03	2.84 ± .14	2.76	1.09	5.32 ± .44	4.90
Cl^{32}	1	1.07	1.62 ± .14	1.51	1.19	1.60 ± .16	1.34
	2	1.05	1.64 ± .25	1.56	1.12	2.04 ± .37	1.82
	3	1.04	2.42 ± .35	2.32	1.10	2.28 ± .34	2.07
	4	1.03	3.00 ± .39	2.92	1.09	1.75 ± .36	1.60

compares the calculated with the measured values of the ratio ${}_{E}T_{A}/{}_{E}T_{B}$ and lists the resulting values of ${}_{E}R_{A,B}$. The calculated values were obtained from the tables of γ-ray absorption coefficients of Davisson and Evans (7). It is seen that ${}_{1}R_{3,5}$ for P^{28} is approximately 2, and for Cl^{32} approximately 1.5. These values increase with E, and at $E = 4$ they become 2.8 and 3, respectively. $R_{5,10}$ values are still higher for P^{28}, but remain essentially the same as $R_{3,5}$ values for Cl^{32}. For Al^{24}, only the $R_{3,5}$ values are significantly different from unity.

No corrections were applied for absorption of β-particles in the target sources.

DISCUSSION OF RESULTS

The general isotopic data listed in Table I are in satisfactory agreement with those given by Glass *et al.* (9). Within the experimental errors all values agree with theirs, and only in the case of the half-life of Cl^{32} are the combined uncertainties needed to give agreement. Birge (4) obtained a value of 2.3 ± .2

sec. for the half-life of Al^{24}, but again there is agreement with the value of Table I within the combined experimental errors.

The γ-rays observed with the three isotopes have been separated into two categories, and are listed in Table VI. Gamma-rays, the peak assignments of

TABLE VI

GAMMA-RAY TRANSITIONS OBSERVED WITH THE ISOTOPES (ENERGY IN MEV.)

Classification	Al^{24}	P^{28}	Cl^{32}
A	1.38 ± .04 2.70 ± .06* 4.21 ± .12* 5.37 ± .14* 7.02 ± .20*	1.78 ± .04† 2.67 ± .08 4.63 ± .10† 4.89 ± .09 6.65 ± .11 7.10 ± .12†	2.25 ± .04 4.33 ± .09 4.82 ± .08*
B	5.66 ± .18	3.01 ± .07 4.26 ± .12 5.16 ± .12† 5.46 ± .10 7.44 ± .14† 7.73 ± .14 8.12 ± .21	3.79 ± .08

* *Also observed by Glass, Jensen, and Richardson (9).*
† *Observed by Casson (6) in* Si^{28}.

which appear to be unambiguous, are included in category *A*. The peak assignments of the γ-rays of category *B* are less certain.

Energy level diagrams showing the lower excited states of Mg^{24}, Si^{28}, and S^{32}, as reported by various observers, are drawn in Fig. 7. The level values are essentially those given in a compilation by Alburger and Hafner (1) with alterations to include more recent experimental work. Hausman *et al.* (10)

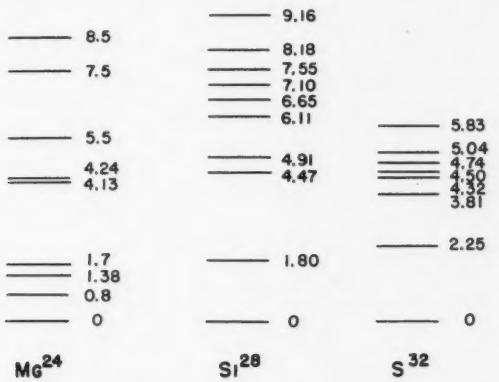

FIG. 7. Energy level diagrams showing the lower energy levels of Mg^{24}, Si^{28}, and S^{32}. The information on these levels has been taken from the literature.

have observed levels in Mg^{24} at 4.13 and 4.24 Mev., in place of the single level at 4.14 Mev. previously thought to exist. In the case of S^{32}, reference was made to the work of Arthur *et al.* (3).

Reference to Table VI shows that the 1.38 Mev. γ-ray with Al^{24} corresponds to a transition between the 1.38 Mev. level and the ground state in Mg^{24}. In fact, in the decay of Na^{24} to Mg^{24}, the presence of 1.38 and 2.75 Mev. γ-rays is well known (11). It is probable that the 2.70 Mev. γ-ray here observed corresponds to the 2.75 Mev. γ-ray. The 4.21 Mev. γ-ray would energetically fit a transition between the 4.24 level and ground state. Glass *et al.* (9) also have observed the γ-rays here marked with an asterisk.

The existence of the 1.80 Mev. level in Si^{28} is confirmed by the presence of a 1.78 Mev. γ-ray in the decay of Al^{28} to Si^{28} (11). It is probable that the 1.78 Mev. γ-ray of P^{28} represents a transition from the same level to the ground state. The 2.67 Mev. γ-ray would energetically fit a transition between the 4.47 and 1.80 Mev. levels in Si^{28}, while the last three γ-rays of group *A* would similarly fit transitions between known levels and the ground state.

It is interesting to compare the spectrum obtained by Casson (6) in a recent study of the γ-rays of resonance capture of protons in Al^{27}, with that of the γ-rays of P^{28}. There is a similarity in these spectra arising in the common excited Si^{28} since three main groups of peaks are present in each case, and within the experimental errors a number of the components are of the same energies. The γ-rays corresponding to these are indicated with a dagger in Table VI. Within the combined experimental errors the 2.67 Mev. γ-ray could also be included in this group.

In the case of Cl^{32}, the γ-rays would energetically fit as transitions between known excited levels in S^{32} and the ground state. However, in view of the background radiation, the experimental evidence for the existence of a 3.79 Mev. γ-ray is uncertain. The presence of the 4.82 Mev. γ-ray is confirmed by the observations of Glass *et al.* (9). Indeed, Glass has stated in a private communication to one of the authors that the agreement is more general than has been indicated above.

The evidence presented suggests that β-particles are present in the decays. In P^{28} and Cl^{32} the values of $R_{A,B}$ are greater than unity, indicating that the reduction in the recorded activity is greater than can be accounted for by the absorption of γ-rays alone. In Al^{24} only the $R_{3,5}$ values differ significantly from unity. It may be that the majority of β-particles from Al^{24} are of lower energy than in the other cases and are almost completely absorbed by the 5 Mev. absorber.

Although only a partial identification of observed γ-transitions with the known levels is possible at this time, sufficient agreement is obtained in each case as to leave little doubt that the new isotopes have been correctly assigned.

ACKNOWLEDGMENTS

The authors wish to acknowledge discussions with Dr. J. D. Jackson and Dr. R. E. Bell. The assistance given by Dr. A. L. Thompson in the preparation of some of the targets, and by Mr. R. H. Mills in the operation of the cyclotron is also much appreciated.

REFERENCES

1. ALBURGER, D. E. and HAFNER, E. M. Revs. Mod. Phys. 22: 373. 1950.
2. ALVAREZ, L. W. Phys. Rev. 75: 1815. 1949; 80: 519. 1950.
3. ARTHUR, J. C., ALLEN, A. J., BENDER, R. S., HAUSMAN, H. J., and MCDOLE, C. J. Phys. Rev. 88: 1291. 1952.
4. BIRGE, ANN C. Phys. Rev. 85: 753. 1952.
5. BRECKON, S. W., MARTIN, W. M., HENRIKSON, A., and FOSTER, J. S. Royal Society of Canada, Paper No. 52, Section III, June Meeting, 1953.
6. CASSON, H. Phys. Rev. 89: 809. 1953.
7. DAVISSON, C. M. and EVANS, R. D. Revs. Mod. Phys. 24: 79. 1952.
8. ELMORE, W. C. and SANDS, M. Electronics, experimental techniques. McGraw-Hill Book Company, Inc., New York. 1949.
9. GLASS, N. W., JENSEN, L. K., and RICHARDSON, J. R. Phys. Rev. 90: 320. 1953.
10. HAUSMAN, H. J., ALLEN, A. J., ARTHUR, J. S., BENDER, R. S., and MCDOLE, C. J. Phys. Rev. 88: 1296. 1952.
11. HOLLANDER, J. M., PERLMAN, I., and SEABORG, G. T. Revs. Mod. Phys. 25: 469. 1953.
12. LI, C. W. Phys. Rev. 88: 1038. 1952.
13. MANDEVILLE, C. E. Phys. Rev. 76: 436. 1949.
14. MARTIN, W. M. and BRECKON, S. W. Can. J. Phys. 30: 643. 1952.
15. WATKINS, D. A. Rev. Sci. Instr. 20: 495. 1949.

FINE STRUCTURE OF THE $F^{19}(\gamma, n)F^{18}$ ACTIVATION CURVE[1]

By J. G. V. Taylor, L. B. Robinson,[2] and R. N. H. Haslam

ABSTRACT

The activation curve for the reaction $F^{19}(\gamma, n)F^{18}$ has been re-examined in great detail up to an energy of 17 Mev. It shows discontinuities which are interpreted as being due to the excitation of discrete nuclear levels. The reaction cross section is discussed on the basis of this curve.

INTRODUCTION

The activation curve for the reaction $F^{19}(\gamma, n)F^{18}$ has been measured in this laboratory by Horsley, Haslam, and Johns (5). The curve was obtained by irradiating LiF powder in the X-ray beam of the betatron, and counting the resulting 112-min. positron activity. The cross section derived from analysis of this curve is shown by the dotted line in Fig. 1. Its shape is unusual in

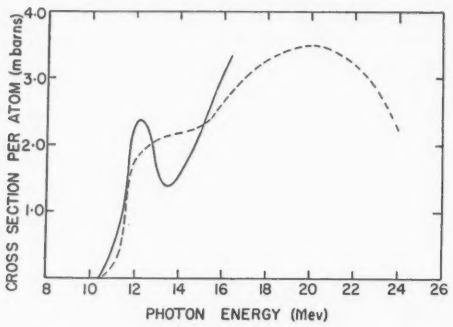

FIG. 1. Cross section for the reaction $F^{19}(\gamma, n)F^{18}$. The heavy line shows the cross-section curve determined in the present work, the dotted line the previously reported cross section (5).

that after a very rapid rise it levels off at 12 Mev., and then rises sharply again at about 15 Mev. The authors concluded that the anomalous shape of the curve must be explained in terms of the X-ray absorption mechanism. In the present paper we report a more detailed examination of the initial portion of the activation curve. Recent improvements in betatron circuitry have made it possible to hold the operating energy stable to $\pm$ 5 kev., and this has made the more detailed examination feasible.

EXPERIMENTAL

In preliminary experiments, NaF samples were pressed into a cylindrical form and counted around Victoreen thyrode tubes. Difficulties were ex-

[1] *Manuscript received November 16, 1953.*
Contribution from the Department of Physics, University of Saskatchewan, Saskatoon, Sask.

[2] *Holder of a National Research Council of Canada bursary, 1953–54.*

perienced due to small quantities of impurities and to the 15 hr. activity induced by the reaction $Na^{23}(n, \gamma)Na^{24}$.

It was found possible to obtain a pure F^{18} activity by using samples of Teflon (polytetrafluoroethylene). The only unwanted activity present is the 20 min. activity of C^{11} produced by the reaction $C^{12}(\gamma, n)C^{11}$. This reaction has a threshold energy of 18.7 Mev., and is thus not produced in the energy region studied.

In a typical experiment, small Teflon samples 2 cm. square and 2 mm. thick were irradiated at a distance of 1 cm. from the donut wall. The induced activity was then counted using two R.C.L. end-window tubes connected in parallel and placed on either side of the sample. Corrections were applied for variation in dose, radiation time, and counting time.

It has been found that the betatron energy is slightly affected by the temperature of the magnet. In order to avoid running over a large temperature range, due to the heat developed by the betatron, each sample was given several short radiations, the betatron magnet being kept within a small temperature range. Even with this precaution, the betatron energy has been observed to shift as much as 100 kv. over a period of several hours after the circuits are turned on. For this reason, a check on the energy was taken at intervals throughout the day.

To check the energy stability, the reaction $Cu^{63}(\gamma, n)Cu^{62}$ was used. The activity within 2 Mev. of the observed threshold has been found to rise as $(E_0 - E_T)^2$, where E_0 is the operating energy and E_T is the threshold energy. Before each day's run, a copper activation curve was taken over the threshold region using an easily duplicated geometry. Then the energy drift during a day could be detected by determining one point on the activation curve. Owing to the rapid rise of activity with energy, any one check would give the relative operating energy accurate to 10 kev. and a shift as small as 5 kev. could be detected. This procedure was suggested by Birnbaum (2). As an additional precaution against energy shifts influencing the shape of the curve, points in any one run were taken in random order. Also, each energy region of the curve was checked on several different days.

The absolute energy calibration of the betatron is based on the measured threshold of the $F^{19}(\gamma, n)F^{18}$ reaction. The measured masses give the threshold energy as 10.41 Mev. (9). The slope of the betatron energy scale was found by measuring the threshold for the $C^{12}(\gamma, n)C^{11}$ reaction, which is 18.71 Mev. Since the determination of the fluorine threshold position is very tedious, the $Cu^{63}(\gamma, n)Cu^{62}$ threshold was determined relative to the fluorine threshold, and found to lie at 10.72 Mev. In subsequent runs the energy scale was based on a measurement of this threshold.

RESULTS AND DISCUSSION

The activation curve (up to 17 Mev.) is shown in Fig. 2. Finer detail of the low energy part of the curve is shown in Fig. 3. It is observed that the graph consists of straight-line sections with sharp breaks at the indicated energies, which are assumed to be due to the excitation of discrete levels in the F^{19}

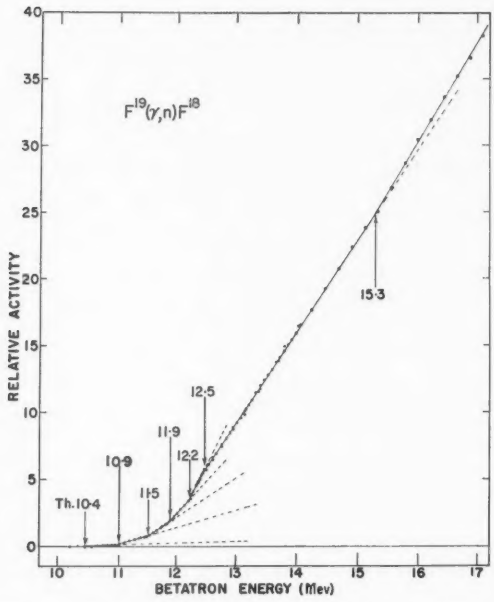

FIG. 2. Activation curve for the reaction $F^{19}(\gamma, n)F^{18}$ showing sharp discontinuities.

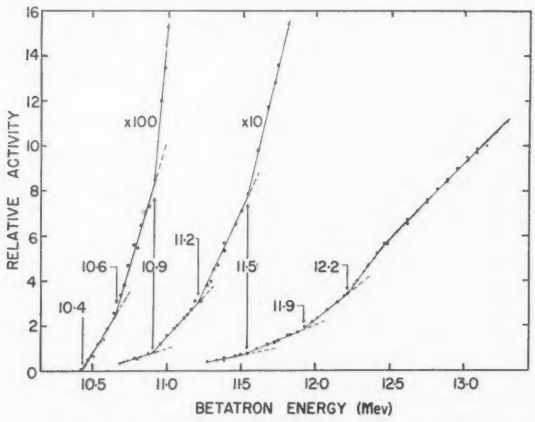

FIG. 3. Finer detail in the low energy section of the $F^{19}(\gamma, n)F^{18}$ activation curve.

nucleus. Work now awaiting publication (8) has established quite clearly that the breaks are not due to any fault of betatron circuitry but are characteristic of the element being irradiated; further, several of the stronger breaks in the $F^{19}(\gamma, n)F^{18}$ activation curve have been confirmed by direct detection of the emitted neutrons. Similar observations have been made previously in the examination of the reaction $O^{16}(\gamma, n)O^{15}$ (4).

It is interesting to note that nuclear levels in the energy region concerned have been found using the reaction $O^{18}(p, n)F^{18}$, which leads to the same compound nucleus and the same residual nucleus (3,10). The results are summarized in the review article by Ajzenberg and Lauritsen (1). Comparison with the results of the present work is made in the accompanying table.

TABLE I

COMPARISON OF NUCLEAR ENERGY LEVELS DETERMINED IN $O^{18}(p, n)F^{18}$ WITH THE POSITIONS OF BREAKS IN THE $F^{19}(\gamma, n)F^{18}$ ACTIVATION CURVE

$O^{18}(p, n)F^{18}$ (Mev.)	$F^{19}(\gamma, n)F^{18}$ (Mev.)
—	10.6
11.0	10.9
—	11.2
11.5	11.5
11.9	11.9
—	12.2
12.7	—
13.2	—
13.7	—
14.2	—
—	15.3

Within the resolution of the experiments three breaks could be identified with previously reported levels; other levels reported were not found in our experiment, perhaps owing to lack of resolution at energies above 12 Mev., or because selection rules forbid the excitation of these levels by photon absorption in F^{19}.

The activation curve (Fig. 2) was analyzed by the photon difference method (7), absolute activity values first being obtained by normalizing to the previously reported curve (5) at 16 Mev. The cross-section curve so calculated is shown by the heavy line in Fig. 1 up to an energy of 16 Mev. A decided maximum is seen to occur at 12.3 Mev.; above 13 Mev. the curve rises again as in the previously reported work.

It is obvious that an analysis of the activation curve making use of $\frac{1}{2}$ Mev. energy intervals (as does the photon difference method for which tables are at present available) must fail to resolve the finer features of the curve. Hence it was thought worth while to analyze the initial portion of the curve by the total spectrum method (6) using 1/10 Mev. steps. The result of such an analysis is shown in Fig. 4. It should be stressed that while the activation curve is in fact reproduced very well by combining this cross-section histogram with the assumed bremsstrahlung spectrum, the cross section is by no means

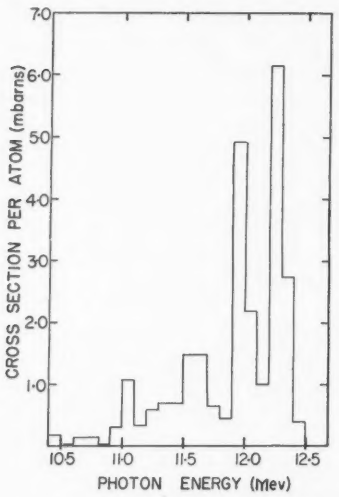

FIG. 4. Cross section resulting from the analysis of the $F^{19}(\gamma, n)F^{18}$ activation curve in 1/10 Mev. energy intervals. This cross section is intended to indicate only the general features of the absorption mechanism.

uniquely determined. This is true for several reasons, the main ones being a lack of knowledge of the exact shape of the 'leading edge' of the bremsstrahlung spectrum, and the lack of resolution in the determination of the activation curve. Further, even if these two difficulties were resolved, only the area under an absorption peak would be determined, and not the height and width separately.

The authors wish to express their thanks to Dr. L. Katz, for valuable discussions, and to R. J. Horsley, D. S. Robb, and J. Goldemberg, who assisted in the determination of the activation curve. The authors are indebted to the National Research Council of Canada for financial support.

REFERENCES

1. AJZENBERG, F. and LAURITSEN, T. Revs. Mod. Phys. 24: 321. 1952.
2. BIRNBAUM, M. Private communication.
3. BLASER, J. P., BOEHM, F., MARMIER, P., and SCHERRER, P. Helv. Phys. Acta, 24: 465. 1951.
4. HASLAM, R. N. H., KATZ, L., HORSLEY, R. J., CAMERON, A. G. W., and MONTALBETTI, R. Phys. Rev. 87: 196. 1952.
5. HORSLEY, R. J., HASLAM, R. N. H., and JOHNS, H. E. Phys. Rev. 87: 756. 1952.
6. JOHNS, H. E., KATZ, L., DOUGLAS, R. A., and HASLAM, R. N. H. Phys. Rev. 80: 1062. 1950.
7. KATZ, L. and CAMERON, A. G. W. Can. J. Phys. 29: 518. 1951.
8. KATZ, L. and GOLDEMBERG, J. Can. J. Phys. 32: 49. 1954.
9. LI, C. W. Phys. Rev. 88: 1038. 1952.
10. RICHARDS, H. T., SMITH, R. V., and BROWNE, C. P. Phys. Rev. 80: 524. 1950.

REFRACTIVE INDEX NOMOGRAM FOR DRY AND HUMID AIR[1]

By P. A. Bricout[2]

ABSTRACT

The refractive index of humid air is the sum of unity plus a term depending on pressure and temperature (dry air refractivity) plus another term dependent on temperature and relative humidity (vapor refractivity). Two alignment nomograms give the values of both refractivities within a range of 300 to 1100 mb. for pressure, +45° C. to −40° C. for temperature, 0 to 100% for relative humidity. Relative errors do not exceed 1% of $(n - 1)$.

An accurate value of the refractive index n of air is needed for optical and hertzian ray tracing in the atmosphere. n differs from unity by only a few ten-thousandths and the value of refractivity $(n - 1)$ depends only on the temperature, pressure, and vapor content of air.

For dry air, $(n - 1)$ varies as the pressure and as the reciprocal of the absolute temperature. In a recent paper discussing previous measurements, Smith and Weintraub (3) have given for the most probable value of the refractivity

$$(n - 1)_a = (ap/T) \times 10^{-6}$$

where $a = 77.6$ if p is measured in millibars and T in Kelvin degrees.

On the alignment nomogram (Fig. 1), $(n - 1)_a$ is read in millionths at the intersection of the oblique *left* scale with a line drawn between points representing pressure and temperature on equidistant scales.

If water vapor is present, its refractivity

$$(n - 1)_v = (bf/T^2) \times 10^{-6},$$

where f is the vapor pressure in millibars, has to be added to that of dry air. Outside of absorption bands of water where anomalous refraction occurs, the classical value given by Kerr (2)

$$b = 3.8 \times 10^5$$

has to be modified to take account of Waynick's (4) and Essen and Frome's (1) measurements.

Smith (3) gives as the most probable value

$$b = (3.73 \pm 0.03) \times 10^5.$$

Assuming this value, the right nomogram (Fig. 1) gives $(n - 1)_v$ by drawing a straight line through the temperature read on the *nonequidistant* scale and through the value of the relative humidity.

As the vapor pressure is very small under the freezing point, a smaller nomogram has been drawn below the main one and should be used below +10° C.

[1] *Manuscript received October 8, 1953.*
Private communication.
[2] *Present Address: 40 Golf Ave., Pointe Claire, Montreal 33, Que.*

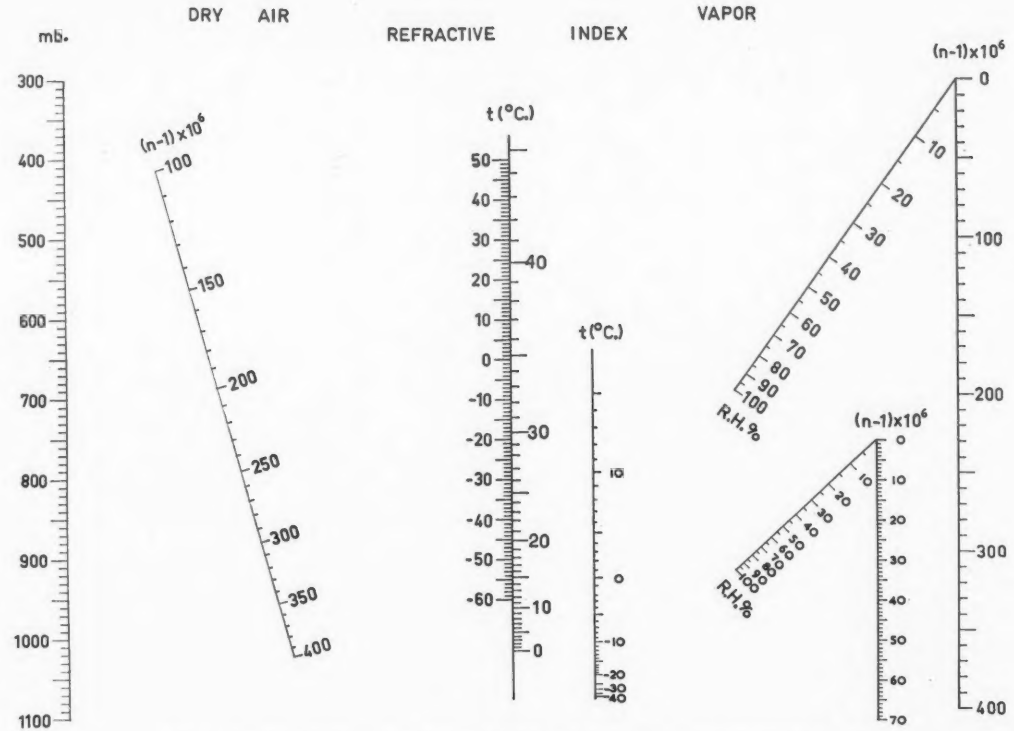

FIG. 1. Alignment nomogram giving (*a*) dry and (*b*) water vapor refractive indices.

Both refractivities are obtained from the most recent values with a relative error not in excess of 1%. They are to be added in the case of humid air.

Example: $p = 950$ mb., $t = +25°$ C., R.H. $= 70\%$.

$(n-1)_a = 247\times10^{-6}$, $(n-1)_v = 92\times10^{-6}$. Humid air: $n - 1 = 339\times10^{-6}$.

REFERENCES

1. ESSEN, L. and FROME, K. D. Proc. Phys. Soc. (London), B, 64: 862. 1951.
2. KERR, D. E. M.I.T. Radiation Laboratory. Vol. 13. McGraw-Hill Book Company, Inc., New York. 1951. p. 189.
3. SMITH, E. K. and WEINTRAUB, S. Proc. I.R.E. 41: 1035. 1953.
4. WAYNICK, A. H. Proc. I.R.E. 28: 468. 1940.

THE EMISSION SPECTRUM OF ALUMINUM MONOFLUORIDE. II[1]

By S. M. Naudé and T. J. Hugo

ABSTRACT

Four new band systems of the emission spectrum of AlF are described, viz. the $D^1\Delta - A^1\Pi$ system in the yellow-green, the $F^1\Pi - A^1\Pi$ and $G^1\Sigma - A^1\Pi$ systems in the blue, and the $F^1\Pi - B^1\Sigma$ system in the infrared spectral region. A vibrational as well as a rotational analysis of the $D^1\Delta - A^1\Pi$ system is reported. The rotational analyses of the other systems, each of which consists of a single band, are described.

A. INTRODUCTION

In a previous paper (5) the $A^1\Pi - X^1\Sigma^+$ and $C^1\Sigma - A^1\Pi$ band systems of the emission spectrum of AlF were described and the analyses reported. In this paper four new singlet systems are described.

These systems were excited according to the method described previously (5) and were also photographed on the 21-ft. grating of the Physics Department, University of Stellenbosch. These systems are considerably weaker than the $A^1\Pi - X^1\Sigma^+$ and $C^1\Sigma - A^1\Pi$ systems and it was essential to minimize the continuous radiation entering the spectrograph slit in order to obtain spectrograms with the necessary contrast.

B. THE $D^1\Delta - A^1\Pi$ SYSTEM

(1) *Vibrational Analysis*

This system consists of three sequences of double-headed bands degraded to the violet. Only the first band of the central sequence at 5773.7Å could be observed because the other bands in this sequence are overlapped by another system of extremely strong and complex bands in the yellow-green. A third order spectrogram of this band, which also shows the overlapping system, is reproduced in Fig. 1. The other two sequences which are very much weaker than the central sequence consist of two bands each.

The rotational structure of these five bands was well resolved in the third order of the grating and the rotational analyses were carried out. The band origins were determined graphically using Q-branch data. In Table I the wave lengths, wave numbers, and estimated intensities of the P-heads as well as the wave numbers of the origins are given. The following equation gives the wave numbers of the band origins of this system:

$$\sigma = 17279.0_1 + [900.68\ (v' + \tfrac{1}{2}) - 5.9_4\ (v' + \tfrac{1}{2})^2] - [804.6_0\ (v'' + \tfrac{1}{2}) - 6.3_3\ (v'' + \tfrac{1}{2})^2]\,.$$

From this equation and from the vibrational combinations it is clear that this system has its lower electronic state in common with the $C^1\Sigma - A^1\Pi$

[1] *Manuscript received December 8, 1953.*
Contribution from the National Physical Laboratory, Council for Scientific and Industrial Research, Pretoria, Union of South Africa.
The work described in the present paper was carried out by one of us (T.J.H.) in part fulfillment of the requirements for the D.Sc. degree of the University of Stellenbosch.

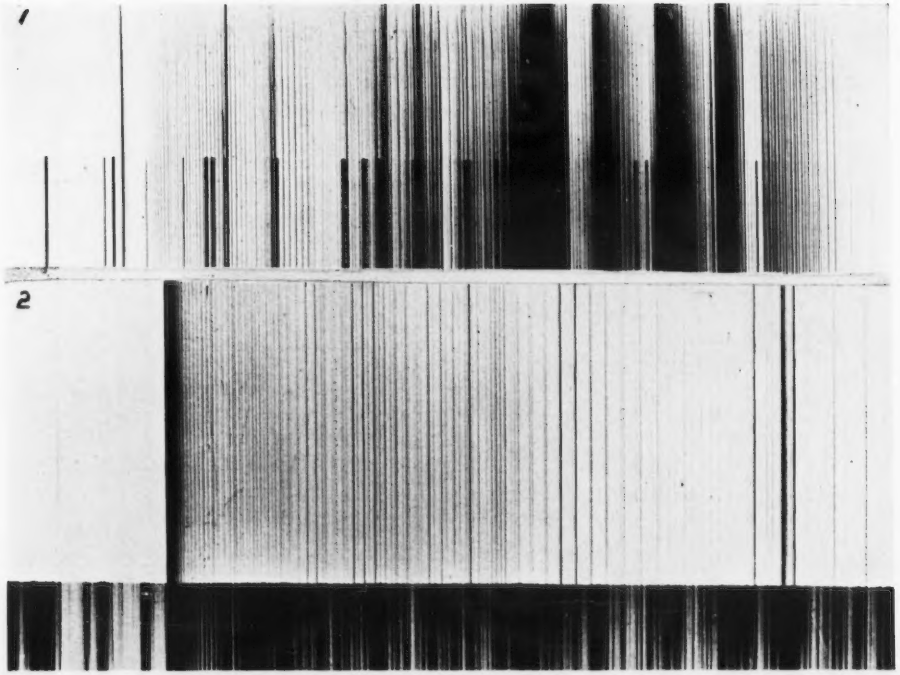

FIG. 1. Third order spectrogram of the (0,0) band of the $D^1\Delta - A^1\Pi$ system and of the complex yellow-green system of AlF.

FIG. 2. Third order spectrogram of the $F^1\Pi - A^1\Pi$ system.

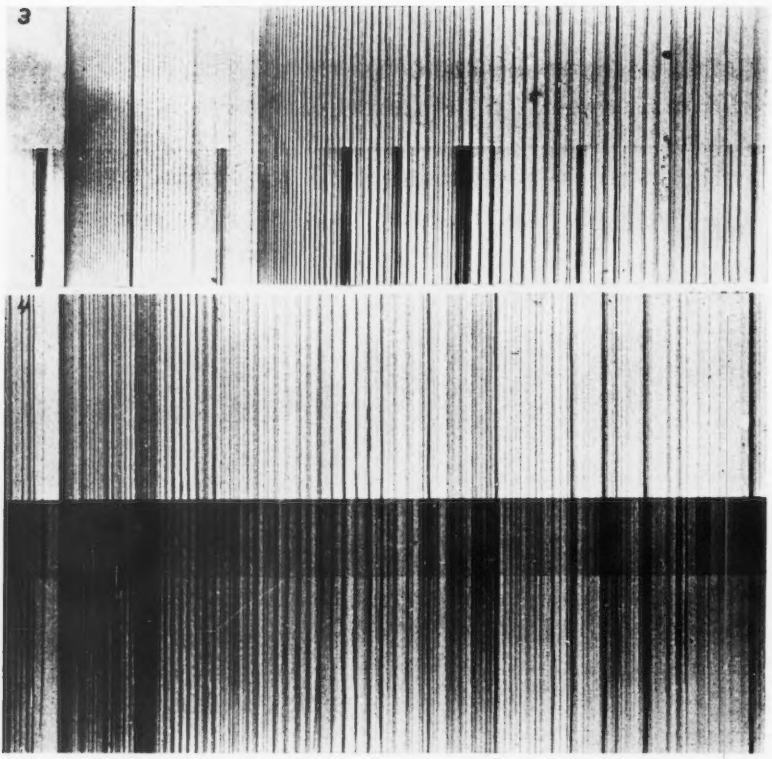

FIG. 3. Second order spectrogram of the $F^1\Pi - B^1\Sigma$ system.
FIG. 4. Third order spectrogram of the $G^1\Sigma - A^1\Pi$ system.

TABLE I

BAND HEAD DATA AND BAND ORIGINS OF THE $D^1\Delta - A^1\Pi$ SYSTEM OF AlF

Wave length of P-head in Å	Wave number of P-head in kaysers	Wave number of origin in kaysers	Intensity	Assignment
6049.6	16525.4	16535.23	2	0,1
6009.7	16635.3	16644.74	1	1,2
5773.7	17315.1	17327.14	10	0,0
5492.6	18201.4	18215.95	1	1,0
5466.9	18286.8	18300.95	0	2,1

system for which the band origins are given by the equation

$$\sigma = 13739.55 + [938.39\ (v' + \tfrac{1}{2}) - 5.18\ (v' + \tfrac{1}{2})^2] - [804.63\ (v'' + \tfrac{1}{2}) - 6.34\ (v'' + \tfrac{1}{2})^2]\,.$$

A summary of the vibrational constants of this system is given in Table II.

TABLE II

VIBRATIONAL AND FORCE CONSTANTS* OF THE $D^1\Delta$ AND $A^1\Pi$ STATES OF AlF

Constant	$A^1\Pi$	$D^1\Delta$
σ_e	43947.0	$17279.0_1 + 43947.0$
σ_{00}	43948.4	$17327.1_4 + 43948.4$
ω_e	804.63	900.68
ω_0	798.29	894.74
$\omega_e x_e$	6.34	5.94
k_e	4.251×10^5	5.326×10^5

* *Conversion factors were obtained from "Spectra of diatomic molecules", 2nd ed., by Gerhard Herzberg.*

The constants of the $A^1\Pi$ electronic state listed in the table are those derived from the $C^1\Sigma - A^1\Pi$ system because of the higher accuracy attained in that system.

(2) *Rotational Analysis*

The third order spectrograms revealed the presence of three branches at low rotation, viz. weak P and R branches and an intense Q branch. At high rotation these branches split into two component branches having the same intensity, thereby indicating a $^1\Delta - {}^1\Pi$ transition.

The vibrational analysis of this system has shown the lower state to be the $A^1\Pi$ state. The upper state is, according to the observed spectrum, the fifth singlet state so that this system is most probably the $D^1\Delta - A^1\Pi$ system of AlF.

In Table III the wave numbers of the lines of the (0,0) and (0,1) bands are given. In Table IV the average $\Delta_2F''(J)$ values for the $v'' = 0$ vibrational state as determined from the $C^1\Sigma - A^1\Pi$, $D^1\Delta - A^1\Pi$, $F^1\Pi - A^1\Pi$, and $G^1\Sigma - A^1\Pi$ systems are compared. The $\Delta_2F'(J)$ values for the $v' = 0$ vibrational state as obtained from the (0,0) and (0,1) bands of the $D^1\Delta - A^1\Pi$ system are

TABLE III

WAVE NUMBERS IN KAYSERS OF THE LINES OF THE (0,0) AND (0,1) BANDS OF THE $D^1\Delta - A^1\Pi$ SYSTEM OF AlF

J	(0,0) band $\lambda_{head} = 5773.7$Å					(0,1) band $\lambda_{head} = 6049.6$Å			
	R_c	R_d	Q_{dc}	Q_{cd}	P	R	Q_{dc}	Q_{cd}	P
3				17327.43					
4				27.62				16535.97	
5				27.89				36.25	
6				28.22				36.63	
7				28.58				37.08	
8				29.01				37.62	
9				29.48				38.17	16549.82
10				30.03	17342.80			38.83	51.58*
11				30.61	44.50			39.53	53.45
12				31.25	46.33			40.31	55.38
13				31.95	48.18			41.31	57.39
14				32.69	50.09			42.00	59.45
15				33.49	52.01			43.00	61.49*
16				34.36	54.06			44.05	63.13
17				35.26	56.13			45.14	66.00
18				36.24	58.24			46.31	68.31
19				37.24	60.43			47.82	70.69
20				38.32	62.67	16525.58*		48.82	—
21				39.44	64.88	25.80		50.17	75.64
22				40.62	67.25	26.07		51.58*	78.22*
23				41.85	69.64	26.39		53.07	80.79
24		17315.33		43.15	72.07	26.78		54.62	83.54
25		15.53		44.50	74.56	27.25		56.24	86.30
26		15.77		45.87	77.12	27.77		57.91	89.12
27		16.08		47.32	79.69	28.37		59.66	92.03
28		16.42		48.82	82.37	29.02		61.49*	94.99
29		16.84		50.39	85.09*	29.77		63.33	95.03
30		17.29		52.01	87.86*	—		65.28	16001.12*
31		17.80		53.66	90.58*	31.41		67.29*	04.24*
32		18.36		55.36*	93.52*	32.35		69.36*	07.51*
33		18.99	57.19*	57.07*	96.44*	33.34		71.47	10.80*
34		19.68*	59.04	58.91	99.42*	34.42		—	14.12*
35		20.40*	60.91	60.77	17402.43*	35.50*		75.94*	17.54*
36	21.26	21.15	62.86	62.67	—	36.63*		78.22*	20.98*
37	22.12	22.00	64.88	64.71	08.65*			80.62*	24.67*
38	23.03	22.89	66.90	66.76	11.79*		83.19*	83.09*	28.24*
39	23.97	23.81	69.02	68.85			85.74*	85.60*	31.80*
40	25.02	24.84	71.19	71.01			88.32	88.20	
41	26.09	25.90	73.40	73.23			91.00	90.85	
42	27.23	27.06	75.68	75.50			93.74	93.55	
43	28.42	28.22	77.99	77.81			96.53	96.37	
44	—	29.48*	80.39	80.16			99.39	99.23	
45	30.98	30.75	82.81	82.62			16602.35	16602.16	
46	32.32	32.09	85.32	85.09			05.36	05.16	
47	33.75	33.49*	87.86	87.61			08.44	08.22	
48	—		90.58	90.24			—	—	
49			93.16	92.90			14.77	14.54	
50			95.87	95.62			18.02	17.81	
51			98.64	98.39			21.37	21.11	
52			17401.49	17401.22			24.67*	—	
53			04.36	04.12			28.04	—	
54			07.32*	07.02			31.53	—	
55			10.33	10.04*					
56									
57									
58									

**Lines marked with an asterisk could not be measured accurately.*

TABLE IV

AVERAGE $\Delta_2F_c''(J)$ VALUES IN KAYSERS OF THE $v = 0$ VIBRATIONAL STATE AS OBTAINED FROM THE $C^1\Sigma - A^1\Pi$ AND $D^1\Delta - A^1\Pi$ BAND SYSTEMS

J	$\Delta_2F_c''(J)$ from the $C^1\Sigma - A^1\Pi$ transition	$\Delta_2F_c''(J)$ from the $D^1\Delta - A^1\Pi$ transition	$\Delta_2F_c''(J)$ from the $F^1\Pi - A^1\Pi$ transition	$\Delta_2F_c''(J)$ from the $G^1\Sigma - A^1\Pi$ transition
10	23.25	23.28		
11	25.51	25.47		
12		27.67		
13		29.89		
14		32.10		
15		34.28		
16		36.49		
17		38.69		
18		40.89		
19		43.14		
20	45.41	45.35		
21	47.56	47.53		47.56
22	49.76	49.75		49.75
23	51.95	51.95	51.74*	51.93
24	54.12	54.12	54.10	—
25	56.34	56.33	56.35	56.40
26	58.54	58.51	58.61	58.57
27	60.74	60.73	60.74	60.73
28	62.97	62.92	62.91	62.96
29	65.11	65.09	65.10	65.18
30	67.31	67.28	67.28	67.34
31	69.48	69.46	69.48	69.57
32	71.70	71.61	71.66	71.83
33	73.89	73.83	73.85	73.91
34	76.02	76.02	76.04	76.01
35	78.24	78.20	78.26	—
36	80.41	80.42	80.43	80.32
37	82.56	82.59	82.61	82.53
38	84.78	84.78	84.76	84.76
39	86.95	86.93	86.98	86.95
40	89.17	89.10	89.08	—
41	91.34	91.27	91.30	91.39
42	93.48	93.43	93.51	
43	95.65	95.45*	95.67	
44	97.79	97.81	97.84	
45	99.94	99.93	99.94	
46	102.11	102.11	102.14	
47	104.24	104.30	104.31	
48	106.46	106.40	106.47	
49	108.58	108.57	108.61	
50	110.73	110.72	110.76	
51	112.93	112.93	112.92	
52	115.05		115.17	
53	117.22		117.21	
54	119.37		119.46	
55	121.48		121.50	
56	123.61		123.61	
57	125.61*		125.78	
58	128.01*		127.87	
59	129.99		130.00	
60	132.10*		132.15	
61	134.21		134.24	
62	136.36		136.35	
63				
64				
65				

TABLE V

$\Delta_2F'(J)$ VALUES IN KAYSERS OF THE $v = 0$ VIBRATIONAL LEVEL OBTAINED FROM THE (0,0) AND (0,1) BANDS OF THE $D^1\Delta - A^1\Pi$ SYSTEM

J	$\Delta_2F'(J)$		J	$\Delta_2F'(J)$	
	(0,0)	(0,1)		(0,0)	(0,1)
10	—	24.40	29	68.26	68.24
11	26.66	26.67	30	70.57	70.56
12	28.97	28.99	31	72.80	72.84
13	31.31	31.15	32	75.13	75.13
14	33.63	33.53	33	77.45	77.44
15	35.92	35.94	34	79.75	79.72
16	38.22	38.17	35	82.03	82.04
17	40.57	40.54	36	84.30	84.35
18	42.87	42.86	37	86.60	86.81*
19	45.19	45.17	38	88.88	89.10*
20	47.54	47.61	39	91.22	91.23
21	49.79	49.88	40	93.49	—
22	52.09	52.15	41	95.77	—
23	54.42	54.43	42	98.02	—
24	56.75	56.74	43	100.27	—
25	59.03	59.05	44	102.55	—
26	61.33	61.35	45	104.85	—
27	63.62	63.67	46	107.12	—
28	65.94	65.96			

given in Table V. The Δ_2F values were obtained from the following equations:

$$\begin{aligned}\Delta_2F'(J) &= R_{e(d)}(J) - P_{e(d)}(J)\\ &= R_{e(d)}(J-1) - Q_{e(d)}(J-1) + R_{e(d)}(J) - Q_{e(d)}(J)\\ &= Q_{e(d)}(J) - P_{e(d)}(J) + Q_{e(d)}(J+1) - P_{e(d)}(J+1)\end{aligned}$$

and

$$\begin{aligned}\Delta_2F''_{e(d)}(J) &= R_{e(d)}(J-1) - P_{e(d)}(J+1)\\ &= R_{e(d)}(J-1) - Q_{e(d)}(J) + R_{e(d)}(J) - Q_{e(d)}(J+1)\\ &= Q_{e(d)}(J-1) - P_{e(d)}(J) + Q_{e(d)}(J) - P_{e(d)}(J+1)\,.\end{aligned}$$

In using the above combinations it is assumed that the Λ-type doubling in the $^1\Delta$ state is negligibly small. This is quantitatively true because the splitting in the branches at high rotation is, within the experimental error, identical with the Λ-type doubling in the $A^1\Pi$ state as determined from the $C^1\Sigma - A^1\Pi$ system.

The rotational constants were determined graphically from the Δ_2F data according to the procedure described by Herzberg (2). These constants are given in Section F where the rotational constants of all four systems are summarized.

C. THE $F^1\Pi - A^1\Pi$ SYSTEM

This system consists of a single weak band, degraded to the violet with its head at 4562.3Å. A third order spectrogram of this band, which is probably the (0,0) band, is shown in Fig. 2.

The rotational structure consists of four branches of the same intensity, viz. double P and R branches. This structure indicates a $^1\Pi - {}^1\Pi$ transition. The wave numbers of the rotational lines are given in Table VI. From these

TABLE VI

WAVE NUMBERS IN KAYSERS OF THE LINES OF THE (0,0) BAND OF THE $F^1\Pi - A^1\Pi$ SYSTEM

J	R_c	P_c	R_d	P_d
10			21939.66	
11	21940.85		41.71	
12	42.83		43.83	
13	44.89		46.05	
14	47.02		48.33	
15	49.15*		50.71	
16	51.50		53.12	
17	53.80		55.66	
18	56.19		58.27	21914.48
19	58.66		60.96	14.78
20	61.21		63.76*	15.12
21	63.76*		66.52*	15.67
22	66.52*		69.48	16.17
23	69.22		72.50	16.84
24	72.02	21914.78	75.58	17.55
25	74.97*	15.12	78.74	18.35
26	77.88	15.67*	81.99	19.24
27	80.89	16.36	85.30	20.20
28	83.98*	17.14	88.71	21.25
29	87.13	17.98	92.18	22.38
30	90.37	18.88	95.76	23.59
31	93.67*	19.85	99.38	24.89
32	97.06*	20.89	22003.13	26.25
33	22000.50*	22.01	06.93	27.70
34	04.03	23.21	10.82	29.24
35	07.61	24.46	14.78	30.84
36	11.26	25.77	18.81*	32.56
37	14.97	27.18	22.94	34.34
38	18.81*	28.65	27.14	36.20
39	22.65	30.21	31.40	38.13
40	26.60	31.83	35.78	40.16
41	30.63	33.57	40.25	42.27
42	34.71	35.30	44.78	44.45
43	38.86	37.12	49.40	46.74
44	43.07	39.04	54.07	49.15*
45	47.41	41.02	58.84	51.50
46	51.78	43.13	63.72	54.06
47	56.24	45.27	68.63	56.67
48	60.77	47.47	73.67	59.38
49	65.33	49.77	78.76	62.15
50	70.04	52.16	83.93	65.05*
51	74.82*	54.57	89.21	67.98*
52	79.60	57.12	94.54*	70.93*
53	84.51	59.65	99.98	74.12
54	89.48	62.39	22105.46	77.29
55	94.54*	65.05*	11.08	80.56
56	99.66	67.98*	16.74	83.98*
57	22104.84	70.93*	22.49	87.42
58	10.11	73.88	28.35	90.95
59	15.48	76.97	34.25	94.59
60	20.19	80.11	40.27	98.28*
61	26.40	83.33	—	22002.13*
62	31.98	86.67	52.54	06.01
63	37.64	90.05	58.80	09.97
64	43.37		65.12	14.07
65	49.20			18.21
66	55.08			—
67	61.07			

data the origin was determined graphically from the equation

$$R(J-1) + P(J) = 2\sigma_0 + 2(B_v' - B_v'')J^2 - 2(D_v' - D_v'')J^2(J+1)^2.$$

The determination gave a value of 21922.23 K for the origin.

The rotational combinations were obtained from the equations

$$\Delta_2 F'_{e(d)}(J) = R_{e(d)}(J) - P_{e(d)}(J)$$

and

$$\Delta_2 F''_{e(d)}(J) = R_{e(d)}(J-1) - P_{e(d)}(J+1)\,.$$

The combinations of the lower state, given in Table IV, prove that this state is the $A^1\Pi$ state. According to the spectrum observed by the authors the upper state is the sixth singlet state of AlF, and this system would accordingly be designated the $E^1\Pi - A^1\Pi$ system. Barrow (1), however, observed in absorption another unspecified singlet state with a lower energy than the upper $^1\Pi$ state of this system from which it follows that this system is most probably the $F^1\Pi - A^1\Pi$ system of AlF. The $\Delta_2 F'$ values are given in Table VII together with the corresponding combinations of the $F^1\Pi - B^1\Sigma$ system which has its upper state in common with this system. In Table VII the $\epsilon(J)$ values for the

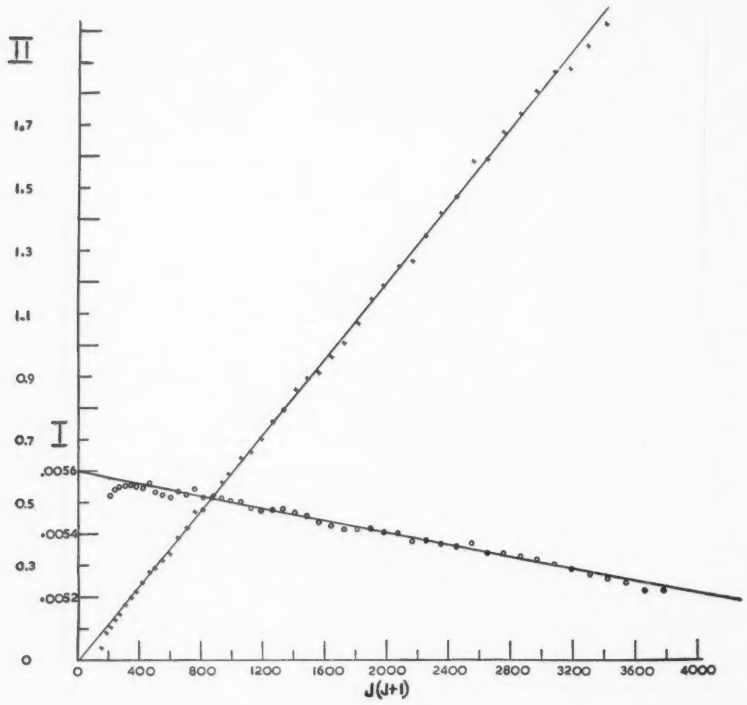

FIG. 5. Graphical determination of the constants for the Λ-type doubling.
I $= \epsilon(J)/2J(J+1)$.
II $= \frac{1}{2}\epsilon(J) - (\mu_c - \mu_d)\,J^2(J+1)^2 - 0.005\,J(J+1)$.

TABLE VII

$\Delta_2F'(J)$ VALUES AND Λ-TYPE DOUBLING OF THE $F^1\Pi$ ELECTRONIC STATE DETERMINED FROM THE $F^1\Pi - A^1\Pi$ AND $F^1\Pi - B^1\Sigma$ SYSTEMS

J	$\Delta_2F_e'(J)$		$\Delta_2F_d'(J)$		$\epsilon(J)$ in $F^1\Pi$	
	From the $F^1\Pi - A^1\Pi$ transition	From the $F^1\Pi - B^1\Sigma$ transition	From the $F^1\Pi - A^1\Pi$ transition	From the $F^1\Pi - B^1\Sigma$ transition	From the $F^1\Pi - A^1\Pi$ transition	From the $F^1\Pi - B^1\Sigma$ transition
9		22.48				
10		—		24.64		
11		27.23		26.99		
12		—		29.32		1.65
13		31.99		31.71		1.99
14		34.38		34.02		2.32
15		36.72		36.38		2.66
16		39.10		38.74		3.02
17		41.47		41.05		3.40
18	43.79	43.84		43.35		3.80
19	46.18	46.19		45.77		4.22
20	48.64	48.53		48.18		4.66
21	50.85	50.93		50.43		5.14
22	53.31	53.33		52.80	5.61	5.60
23	55.66	55.67		55.17	6.03	6.10
24	58.03	58.01	57.24*	57.50	6.61	6.62
25	60.39	60.41	59.67*	59.86	7.25	7.20
26	62.75	62.78	62.21	62.15	7.91	7.76
27	65.10	65.07	64.53	64.49	8.36	8.38
28	67.46	67.46	66.84	66.83	8.95	8.96
29	69.80	69.79	69.15	69.18	9.76	9.60
30	72.17	72.18	71.49	71.51	10.25	10.26
31	74.49	74.54	73.82	73.77	10.93	10.92
32	76.88	76.77	76.17	76.19	11.60	11.62
33	79.23	79.22	78.49	78.49	12.30	12.30
34	81.58	81.55	80.82	80.84	13.03	13.02
35	83.94	83.94	83.15	83.14	13.82	13.80
36	86.24	86.24	85.49	85.47	14.57	14.60
37	88.60	88.56	87.79	87.81	15.36	15.38
38	90.94	90.96	90.16	90.11	16.17	16.18
39	93.27	93.25	92.44	92.40	16.96	16.96
40	95.62	95.54	94.77	94.74	17.77	17.80
41	97.98	97.94	97.06	97.05	18.65	18.65
42	100.33	100.29	99.41	99.36	19.58	19.56
43	102.66	102.61	101.74	101.73	20.54	20.50
44	104.92		104.03	104.03	21.42	
45	107.34		106.39	—	22.33	
46	109.66		108.65		23.25	
47	111.96		110.97		24.27	
48	114.29		113.30		25.23	
49	116.61		115.56		26.27	
50	118.88		117.88		27.32	
51	121.23		120.25		28.22	
52	123.61		122.48		29.40	
53	125.86		124.86		30.40	
54	128.17		127.09		31.56	
55	130.52		129.49		32.58	
56	132.76		131.68		33.65	
57	135.07		133.91		34.81	
58	137.40		136.23		35.95	
59	139.66		138.51		37.11	
60	141.99		140.80		38.29	
61	—		143.07		39.46	
62	146.53		145.31			
63	148.83		147.59			
64	151.05					

TABLE VIII

WAVE NUMBERS OF THE LINES OF THE (0,0) BANDS OF THE $F^1\Pi - B^1\Sigma$ AND $G^1\Sigma - A^1\Pi$ SYSTEMS

J	$F^1\Pi - B^1\Sigma$ $\lambda_{head} = 8648.5$Å			$G^1\Sigma - A^1\Pi$ $\lambda_{head} = 4453.2$Å		
	R	Q	P	R	Q	P
6	11597.73				22458.76*	
7	—				59.35	
8	11600.31	11590.17	11580.41*		60.15*	
9	01.69	90.43	—		60.94	
10	03.05	90.75	78.41		61.90	
11	04.47	—	77.48		62.92	
12	05.88	91.49	76.56		64.07	
13	07.36	91.91	75.65		65.32	
14	08.80	92.38	74.78		66.59*	
15	10.30	92.85	73.92		68.04	
16	11.83	93.39	73.09		69.59	22450.46*
17	13.36	93.96	72.31		71.14	50.83
18	14.86*	94.54	71.51		72.88	51.29
19	16.52	95.17	70.75		74.60*	51.91
20	18.14	95.83	69.96	22501.81	76.58	52.59
21	19.77	96.52	69.34	04.99	78.56	53.39
22	21.43	97.25	68.63	08.29	80.65	54.24
23	23.11	98.02	67.94	11.69	82.80	55.24
24	24.82	98.81	67.32	15.16	85.09	56.36
25	26.57*	99.63	66.71	18.72	87.44	—
26	28.25	11600.50	66.10	22.36	89.93	58.76*
27	30.05	01.40	65.56	26.14	92.47	60.15*
28	31.84	02.33	65.01	30.02	95.12	61.63
29	33.66	03.29	64.48	33.93	97.93	63.18
30	35.51	04.28	64.00	38.00	22500.74	64.84
31	37.28	05.32	63.51	42.21	03.64	66.59*
32	39.27	06.39	63.08	46.31	06.69	68.43
33	41.18	07.50	62.69	50.61	09.80	70.38
34	43.11	08.61	62.27	—	13.02	72.40
35	45.06	09.79	61.92	59.42	16.29	74.60*
36	47.05	11.02	61.58	64.03	19.74	76.80
37	49.07	12.23	61.26	68.79	23.24	79.10
38	51.10	13.52	60.99	73.57	26.84	81.50
39	53.14	14.86*	60.74	78.59	30.49	84.03
40	55.24	16.17	60.50	83.65	—	86.62
41	57.34	17.55	60.29	—	38.27	—
42	59.46	18.97	60.10		42.21	92.26
43	61.65	20.42	59.92		46.31	95.12
44	63.83	21.92	59.80*		50.49	98.14
45	66.03	23.45			54.77	22501.21
46	68.28	24.99			59.11	
47	70.53	—			63.58	
48		28.25*			68.12	
49		29.90			72.77	
50		31.60			77.51	

$F^1\Pi$ state, as determined from the $F^1\Pi - A^1\Pi$ and $F^1\Pi - B^1\Sigma$ systems, are also given. The $\epsilon(J)$ values were determined from the $F^1\Pi - A^1\Pi$ system by assuming that the splitting in the branches gives the difference in the Λ-type doubling in the upper and lower states, i.e. by assuming that the two $^1\Pi$ states have the same symmetry.

For the determination of the doubling from the $F^1\Pi - B^1\Sigma$ system it was assumed (4) that the doubling at $(J + \frac{1}{2})$ is given by the equation:

$$\epsilon(J + \tfrac{1}{2}) = R(J) - Q(J) - Q(J + 1) + P(J + 1) .$$

From the $\epsilon(J + \frac{1}{2})$ data the $\epsilon(J)$ values were determined graphically.

The constants (3) of the Λ-type doubling equation were also determined graphically and the following equation was obtained:

[1] $\frac{1}{2}\epsilon(J) = -0.0000_{05} + 0.0056_{0}\, J(J+1) - 9.8 \times 10^{-8}\, J^2(J+1)^2$.

The graphs for determining the constants in equation [1] are shown in Fig. 5. This equation corresponds well with the equation derived from the rotational constants of the $F^1\Pi$ state given in Tables X and XII, viz.:

$$\tfrac{1}{2}\epsilon(J) = -0.0001_{9} + 0.0057_{9}\, J(J+1) - 1._{15} \times 10^{-7}\, J^2(J+1)^2.$$

D. THE $F^1\Pi - B^1\Sigma$ SYSTEM

This system consists of the weak, double-headed band shown in Fig. 3. The band, probably the (0,0) band, is degraded to the violet and has its long-wave-length head at 8638.6Å.

The rotational structure consists of a strong Q branch and weaker P and R branches. The wave numbers of the lines of the band are given in Table VIII. The origin of the band, determined graphically from Q branch data, is at 11588.87 K.

The rotational combinations for the upper state, given in Table VII, prove this state to be the $F^1\Pi$ state. The lower state is according to the observed spectrum the first electronic state above the $A^1\Pi$ state and the system, therefore, most probably the $F^1\Pi - B^1\Sigma$ system of AlF.

The rotational combinations for the lower state are given in Table IX together with the combinations of the $G^1\Sigma$ state.

TABLE IX

$\Delta_2F(J)$ VALUES IN KAYSERS OF THE $v = 0$ VIBRATIONAL LEVELS OF THE $G^1\Sigma$ AND $B^1\Sigma$ ELECTRONIC STATES OBTAINED FROM THE (0,0) BANDS OF THE $G^1\Sigma - A^1\Pi$ AND $F^1\Pi - B^1\Sigma$ SYSTEMS

J	$\Delta_2F'(J)$ from the $G^1\Sigma - A^1\Pi$ transition	$\Delta_2F''(J)$ from the $F^1\Pi - B^1\Sigma$ transition	J	$\Delta_2F'(J)$ from the $G^1\Sigma - A^1\Pi$ transition	$\Delta_2F''(J)$ from the $F^1\Pi - B^1\Sigma$ transition
7		17.32	27	65.99	63.24
8		—	28	68.39	65.57
9		21.90	29	70.75	67.84
10		24.21	30	73.16	70.15
11		26.49	31	75.62	72.43
12		28.82	32	77.88	74.59
13		31.10	33	80.23	77.00
14		33.44	34	—	79.26
15		35.71	35	84.82	81.53
16		37.99	36	87.23	83.80
17		40.32	37	89.69	86.06
18		42.61	38	92.07	88.33
19		44.90	39	94.56	90.60
20	49.22	47.18	40	97.03	92.85
21	51.60	49.51	41		95.14
22	54.05	51.83	42		97.42
23	56.45	54.11	43		99.66
24	58.80	56.40	44		
25	—	58.72	45		
26	63.60	61.01			

E. THE $G^1\Sigma - A^1\Pi$ SYSTEM

As in the previous two systems, this system consists of a single, double-headed band, degraded to shorter wave lengths, with its head at 4453.7Å. A third order spectrogram of the band, which is probably the (0,0) band, is reproduced in Fig. 4.

The rotational structure consists of a strong Q branch with weaker P and R branches, thus indicating a transition between a $^1\Sigma$ and $^1\Pi$ state. The wave numbers of the lines are given in Table VIII. The origin of the band, determined from the Q branch data, lies at 22456.77 K.

The rotational combinations for the lower state, given in Table II, prove this state to be the $A^1\Pi$ state. According to the observed spectrum, the upper state follows immediately upon the $F^1\Pi$ state. This band system is therefore most probably the $G^1\Sigma - A^1\Pi$ system of AlF.

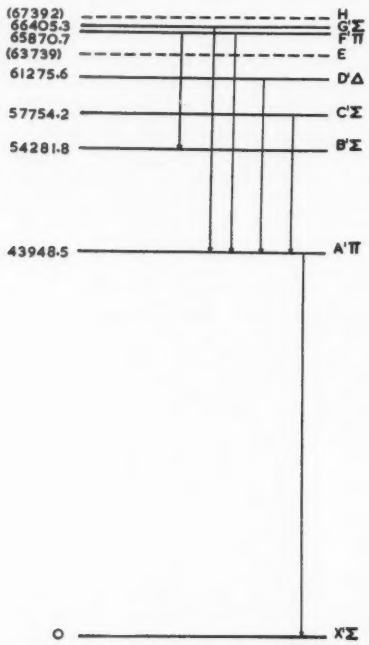

FIG. 6. Diagram of the σ_{00} values of the singlet states of AlF.

In Fig. 6 a diagram is given of the observed electronic energy levels as well as the observed transitions. The two levels indicated by dotted lines were observed by Barrow (1). For the purpose of this diagram the σ_{00} values were assumed to be characteristic of the electronic energy levels.

F. SUMMARY OF ROTATIONAL CONSTANTS

The rotational constants for the different systems are summarized in Tables X–XIII. Equilibrium rotational constants could only be determined for the $A^1\Pi$ and $D^1\Delta$ electronic states. These constants are given in Table XIV.

TABLE X

ROTATIONAL CONSTANTS OF THE $D^1\Delta - A^1\Pi$ SYSTEM

v'	$D^1\Delta$ state		$A^1\Pi_c$ state		$A^1\Pi_d$ state		$A^1\Pi$ state	
	B_v (K)	D_v (K)	$B_v{}^c$ (K)	$D_v{}^d$ (K)	$B_v{}^d$ (K)	$D_v{}^d$ (K)	B_v (K)	D_v (K)
0	0.5801_9	$9._7 \times 10^{-7}$	0.5536_8	$1._{03} \times 10^{-6}$	0.5538_1	$1._{03} \times 10^{-6}$	0.5537_5	$1._{03} \times 10^{-6}$
1	0.5756_3	$1._{10} \times 10^{-6}$	0.5480_0	$1._{04} \times 10^{-6}$	0.5482_1	$1._{04} \times 10^{-6}$	0.5481_1	$1._{04} \times 10^{-6}$
2	0.5704_5	$1._{15} \times 10^{-6}$	0.5438	$1._{08} \times 10^{-6}$	0.5438	$1._{08} \times 10^{-6}$	0.5428	$1._{08} \times 10^{-6}$

TABLE XI

ROTATIONAL CONSTANTS OF THE $F^1\Pi - A^1\Pi$ SYSTEM

v'	$A^1\Pi_c$ state		$A^1\Pi_d$ state		$A^1\Pi$ state	
	$B_v{}^c$ (K)	$D_v{}^c$ (K)	$B_v{}^d$ (K)	$D_v{}^d$ (K)	B_v (K)	D_v (K)
0	0.5537_7	$1._{01} \times 10^{-6}$	0.5538_3	$1._{01} \times 10^{-6}$	0.5538_0	$1._{01} \times 10^{-6}$
v'	$F^1\Pi_c$ state		$F^1\Pi_d$ state		$F^1\Pi$ state	
	$B_v{}^c$ (K)	$D_v{}^c$ (K)	$B_v{}^d$ (K)	$D_v{}^d$ (K)	B_v (K)	D_v (K)
0	0.5875_2	$7._4 \times 10^{-7}$	0.5932_1	$8._9 \times 10^{-7}$	0.5903_7	$8._2 \times 10^{-7}$

TABLE XII

ROTATIONAL CONSTANTS OF THE $G^1\Sigma - A^1\Pi$ SYSTEM

v'	$G^1\Sigma$ state		$A^1\Pi$ state	
	B_v (K)	D_v (K)	B_v (K)	D_v (K)
0	0.692_0	$1._{15} \times 10^{-6}$	0.553_8	$1._{06} \times 10^{-6}$

TABLE XIII

ROTATIONAL CONSTANTS OF THE $F^1\Pi - B^1\Sigma$ SYSTEM

v'	$B^1\Sigma$ state		$F^1\Pi_c$ state		$F^1\Pi_d$ state		$F^1\Pi$ state	
	B_v (K)	D_v (K)	$B_v{}^c$ (K)	$D_v{}^c$ (K)	$B_v{}^d$ (K)	$D_v{}^d$ (K)	B_v (K)	D_v (K)
0	0.5759_8	$9._7 \times 10^{-7}$	0.5873_8	$7._6 \times 10^{-7}$	0.5932_0	$8._4 \times 10^{-7}$	0.5902_9	$8._0 \times 10^{-7}$

TABLE XIV

EQUILIBRIUM ROTATIONAL CONSTANTS OF THE $A^1\Pi$ AND $D^1\Delta$ ELECTRONIC STATES

Electronic state	B_e (K)	D_e (K)	α_e	r_e (Å)
$A^1\Pi$	0.5565_2	1.10×10^{-6}	0.0055_2	1.648
$D^1\Delta$	0.5827_2	1.04×10^{-6}	0.0048_7	1.611

The low intensity of the $G^1\Sigma - A^1\Pi$ band and the resultant short series in the rotational structure prevented an accuracy sufficiently high to distinguish between the $A^1\Pi_c$ and $A^1\Pi_d$ states. Accordingly only the average $A^1\Pi$ value is listed in Table XII.

The equilibrium constants of the $A^1\Pi$ state given in Table XIV were calculated from all the available data on the different singlet systems and correspond to the average value for all the observed systems which have this state as the lower electronic state. The low relative accuracy in the determination of the D_v values does not permit the calculation of reliable D_e values. Accordingly the D_e values in this table are only weighted average D_v values.

G. ACKNOWLEDGMENTS

The authors wish to thank Dr. P. B. Zeeman, promotor of one of us (T.J.H.), for suggesting the problem and Prof. P. de Vos for placing the facilities of the Department of Physics, University of Stellenbosch, at our disposal. We further wish to thank Mr. S. Meier for his help with the experimental work.

This paper is published with the permission of the Council for Scientific and Industrial Research.

REFERENCES

1. BARROW, R. F. Private communication. 1953.
2. HERZBERG, G. Spectra of diatomic molecules. 2nd ed. D. Van Nostrand Company, Inc., New York. 1950. p. 183.
3. HERZBERG, G. Spectra of diatomic molecules. 2nd ed. D. Van Nostrand Company, Inc., New York. 1950. p. 227.
4. MULLIKEN, R. S. and CHRISTY, A. Phys. Rev. 38: 87. 1931.
5. NAUDÉ, S. M. and HUGO, T. J. Can. J. Phys. 31: 1106. 1953.

ON THE CONCEPT OF FIELD QUANTIZATION[1]

By F. A. Kaempffer

ABSTRACT

Attempts by Takabayasi and Kaempffer at an entirely different method of field quantization, starting from the hydrodynamic formulation of classical field theories rather than from their formulation in terms of wave equations, are examined in the light of Ziman's recent successful approach towards the quantum hydrodynamical problem. It is pointed out that the energetic impossibility of a roton spectrum in an ideal continuum fluid, as shown by Ziman, makes it necessary to introduce into the theory a fundamental length, which acts as high frequency cut-off, and which may be interpreted as representing a substructure of the medium in which elementary particles may appear as excitations of the motion. Takabayasi's generalized hydrodynamic formulation of the nonrelativistic Schroedinger equation is treated as an example, and it is shown that the fundamental length must be of the order $\hbar/mc$, if the particle corresponding to the single roton excitation of the Takabayasi field is to have the mass m.

Contemporary theories of elementary particles, particularly the so-called meson theories, are without exception elaborations on an idea of Heisenberg and Pauli (4), published in 1929. The starting point of these theories is the hypothesis that the classical analogue, in the sense of Bohr's correspondence principle, of any many-particle theory is a classical wave theory, derivable from a variational principle

$$[1] \qquad \delta \int L\left(\psi, \frac{\partial \psi}{\partial x_i}, \psi, \ldots\right) d^3x\, dt = 0$$

such that the integral $\int \psi^* \psi\, d^3x$ corresponds to the number of particles present in the quantized form of the theory. This correspondence is, in fact, established if quantization of the classical theory [1] is carried out by postulating for the wave function ψ itself commutation relations of the type

$$[2] \qquad [\psi(x), \psi^*(x')] = \delta(x - x') .$$

The strength of this approach is the mathematical equivalence of the resulting quantum theory with the theory resulting from quantization of a classical many-particle theory (3).

However, quite apart from the well-known and unsolved divergence difficulties, these theories are seriously unsatisfactory inasmuch as with n experimentally known types of elementary particles one has to introduce at least $n(n + 1)/2$ empirical constants into the theory in order to describe all of them, since the nth type of particle must be characterized at least by its mass and by $n - 1$ coupling constants with all the other known types of particles. Thus, with the steadily increasing number of known types of particles, the hope of obtaining a unified theory of elementary particles in terms of conventional quantum field theory is fading rapidly.

To break this deadlock, Takabayasi (8), using a generalization of Bohm's (1) reformulation of quantum mechanics, and Kaempffer (5), using a general-

[1] *Manuscript received October 19, 1953.*
Contribution from the Department of Physics, The University of British Columbia, Vancouver, B.C.

ization of Dirac's (2) new electrodynamics, have made attempts at introducing an entirely different procedure of quantization of classical field theories, starting from hydrodynamic formulations rather than from wave equations, and proposing quantization of the theory along the lines of quantum hydrodynamics, in which the velocity potentials rather than the wave functions are subjected to commutation relations of the type [2]. The aim of these attempts is to obtain a unified theory of elementary particles, in which different types of particles appear as different forms of excitations of the motion of one underlying medium, which is characterized by the field equations, in analogy to the phonons and rotons appearing as quantized excitations of the motion in a nonviscous fluid upon quantization of the classical equations of hydrodynamics.

Although these attempts are still programs rather than complete theories, some light is thrown on their feasibility by Ziman's (9) recent successful approach towards the quantum hydrodynamical problem. Ziman has shown that the classical equations of hydrodynamics for a nonviscous fluid are identical with the canonical equations of motion derived from the Hamiltonian density

$$H = \tfrac{1}{2}\rho\mathbf{u}^2 + W(\rho) \tag{3}$$

where the velocity vector $\mathbf{u}$ is expressed in terms of the density ρ and three potentials ϕ, ψ_1, ψ_2 by

$$\mathbf{u} = -\operatorname{grad}\phi - \frac{1}{2\rho}(\psi_2 \operatorname{grad}\psi_1 - \psi_1 \operatorname{grad}\psi_2), \tag{4}$$

where $W(\rho)$ is the potential energy per unit volume of the fluid, and where (ρ, ϕ) and (ψ_1, ψ_2) are pairs of canonically conjugate variables. The potentials ψ_1 and ψ_2 which characterize the vortex motion of the fluid are connected by a canonical transformation with the well-known Clebsch potentials of hydrodynamics. In order to make the choice of ϕ, ψ_1, ψ_2 unambiguous, Ziman assumes further that ψ_1 and ψ_2 are real and imaginary parts of a complex field function

$$\Psi = (2\hbar)^{-\frac{1}{2}}(\psi_1 + i\psi_2); \quad \Psi^* = (2\hbar)^{-\frac{1}{2}}(\psi_1 - i\psi_2) \tag{5}$$

and carries out the quantization of his theory by postulating the commutation relations

$$[\phi(x), \rho(x')] = i\hbar\delta(x - x'); \quad [\Psi(x), \Psi^*(x')] = \delta(x - x') \tag{6}$$

with all other commutators vanishing. It is then possible to split the total Hamiltonian of the system into terms $\mathfrak{H}_{\text{phon}} + \mathfrak{H}_{\text{interact}} + \mathfrak{H}_{\text{rot}}$ where the part describing the vortex motion alone, $\mathfrak{H}_{\text{rot}}$, upon which we now fix our attention, takes after the usual Fourier transformation

$$\Psi = V^{-\frac{1}{2}}\sum_{\mathbf{k}} b_{\mathbf{k}} e^{i\mathbf{k}\mathbf{x}}; \quad \Psi^* = V^{-\frac{1}{2}}\sum_{\mathbf{k}} b^*_{\mathbf{k}} e^{-i\mathbf{k}\mathbf{x}} \tag{7}$$

the form:

$$\mathfrak{H}_{\text{rot}} = \frac{\hbar^2}{8\rho_0 V} \times \left\{ \sum_{\mathbf{k}}\sum_{\mathbf{l}}\sum_{\mathbf{m}}\sum_{\mathbf{n}} \delta_{\mathbf{k}+\mathbf{l},\mathbf{m}+\mathbf{n}}(\mathbf{k}+\mathbf{n})(\mathbf{l}+\mathbf{m})\, b^*_{\mathbf{m}} b^*_{\mathbf{n}} b_{\mathbf{k}} b_{\mathbf{l}} + \sum_{\mathbf{k}}\sum_{\mathbf{l}} (k^2 + l^2)\, b^*_{\mathbf{k}} b_{\mathbf{k}} \right\}. \tag{8}$$

The eigenvalues of this Hamiltonian can be written down immediately for those states of the fluid in which just one "roton" of propagation vector $\mathbf{k}$ is present:

$$E_{\mathbf{k}} = \frac{\hbar^2}{8\rho_0 V} \sum_{\mathbf{l}} (l^2 + k^2). \tag{9}$$

Since it follows from this expression that vortex motion in an ideal continuum fluid is energetically forbidden, the sum over $\mathbf{l}$ being infinite, Ziman introduces at this stage the atomic substructure of the fluid by cutting off all propagation vectors that correspond to a length shorter than the mean distance between two neighboring atoms in the fluid. In other words, the substructure of the fluid consisting of N atoms is characterized by a shortest length

$$\lambda \cong (V/N)^{1/3}. \tag{10}$$

One obtains then by summation over all $\mathbf{l}$ up to $l_{\max} \sim 1/\lambda$

$$\sum_{\mathbf{l}} l^2 \cong V\lambda^{-5} \tag{11}$$

and the energy of the single roton state takes the form

$$E_{\mathbf{k}} \cong \frac{\hbar^2}{\rho_0 \lambda^5} + \frac{\hbar^2 k^2}{\rho_0 \lambda^3}. \tag{12}$$

It is interesting to note that the first term of this expression may be interpreted as the "rest energy" of a roton, while the second term represents the kinetic energy of a roton of momentum $\mathbf{p} = \hbar\mathbf{k}$. Following a suggestion by Kramers (7) we may then call

$$\mu \cong \rho_0 \lambda^3 \tag{13}$$

the "effective mass" of a roton and write the rest energy in the form μc^2 with

$$c \cong \hbar/\mu\lambda\,. \tag{14}$$

Clearly, in any theory of elementary particles, based upon a classical theory resembling formally the hydrodynamics of a nonviscous fluid, Ziman's theorem regarding the energetic impossibility of a roton spectrum in an ideal continuum fluid will remain valid. It must be concluded that attempts of the type proposed by Takabayasi and Kaempffer can be successful only if a shortest length λ is introduced into the theory, so that excitation of single roton states becomes energetically possible. One may then interpret λ as a fundamental length characteristic for the substructure of the medium in which observable particles may appear as excitations of the motion. In case one wishes to identify this underlying medium with the Dirac sea it is not too hard on the imagination to visualize this substructure as being due to a finite density of the electrons of negative energy (6).

In order to see better how the fundamental length enters the theory, we shall look a bit closer at Takabayasi's attempt in the light of Ziman's quantum hydrodynamics. It is not to be expected that Takabayasi's attempt will yield an entirely satisfactory theory of elementary particles, since it is based upon a generalization of the nonrelativistic Schroedinger equation. One might as well start with similar generalizations of relativistic equations, like the

Klein Gordon equation, and Takabayasi (8) has, in fact, considered such possibilities. Besides, the attempt by Kaempffer, based upon a generalization of Dirac's new electrodynamics, seems more promising, since it offers the prospect of understanding the electromagnetic properties of elementary particles by identification of the momentum vector of the motion with the electromagnetic potentials. But since we are concerned here with a general feature of these attempts, it will suffice to treat Takabayasi's theory only, because it is representative of the new approach, and because its mathematical apparatus resembles most closely Ziman's formalism.

The starting point of Takabayasi (8) is the system of classical equations

$$m\frac{D\mathbf{u}}{Dt} = -\operatorname{grad}\left(V - \frac{\hbar^2}{2m}\frac{\nabla^2 R}{R}\right), \tag{15}$$

$$\frac{\partial P}{\partial t} = -\operatorname{div}(P\mathbf{u}) \tag{16}$$

which are obtained from the nonrelativistic Schroedinger equation upon substitution of

$$\psi = R\exp(iS/\hbar) \tag{17}$$

with $\mathbf{u} = (\operatorname{grad} S)/m$, $P \equiv R^2$, and which may be interpreted, according to a suggestion by Bohm (1), as representing an ensemble of particle trajectories belonging to a velocity potential S. These equations are now generalized so as to include the possibility of vortex motion in the medium by expressing the velocity vector in terms of the scalar potential s and two Clebsch potentials ξ, η

$$\mathbf{u} = -\operatorname{grad} s - \xi \operatorname{grad} \eta\,. \tag{18}$$

Since it is always possible to choose the time dependence of ξ and η such that the vortex-lines move with the fluid, i.e.

$$\frac{D\xi}{Dt} = 0; \quad \frac{D\eta}{Dt} = 0, \tag{19}$$

the equations [15], [16], and [19] form a system which is formally identical with the fundamental equations of Ziman's theory, provided we interpret $mP = \rho$ as density of the Takabayasi field, which is described now in terms of four space-time functions ρ, s, ξ, η. Consequently, these equations may be considered as canonical equations derivable from a Hamiltonian density

$$H = \tfrac{1}{2}\rho\mathbf{u}^2 + U(\rho); \quad U(\rho) = \frac{\rho V}{m} + \frac{\hbar^2}{8}\frac{(\operatorname{grad}\rho)^2}{\rho} \tag{20}$$

and upon Ziman's canonical transformation

$$\eta = \psi_1/\psi_2; \quad \xi = \psi_2^2/2\rho\,, \tag{21}$$

the complete mathematical equivalence of Takabayasi's classical theory with equations [3] and [4] is established. Since $U(\rho)$ does not contribute to the vortex motion of the field, the roton part of the Hamiltonian following from [20] will be exactly the same as [8], if quantization of Takabayasi's theory is carried

out along the lines of quantum hydrodynamics. Accordingly, Ziman's conclusions regarding the impossibility of vortex motion in an ideal continuum fluid and the subsequent surmounting of this obstacle by introduction of a shortest length characteristic for the field can be applied immediately. Thus, single roton states of the Takabayasi field exist, and contribute to the energy of the system, if their momentum is p, the amount

$$E(p) \cong \frac{\hbar^2}{\rho_0 \lambda^5} + \frac{p^2}{\rho_0 \lambda^3}. \tag{22}$$

Now, if one intends to look upon such a roton as an observable particle of mass m, the energy of the roton must be written in the form

$$E(p) = mc^2 + \frac{p^2}{2m}; \qquad c = \text{velocity of light.} \tag{23}$$

We conclude that *single roton states of the Takabayasi field, as far as their contribution to the energy is concerned, behave like particles of mass m, provided a fundamental length of the order*

$$\lambda \cong \hbar/mc \tag{24}$$

is introduced into the theory.

Nothing can be said as yet about possible higher roton states of the Takabayasi field, since this would require complete diagonalization of the roton Hamiltonian [8]. It seems highly desirable that efforts be made to solve this difficult mathematical problem, since its solution should yield the mass spectrum of possible higher roton excitations in terms of the "ground state" of mass m. In addition, a large number of other questions have to be answered before one may call this approach a successful one. Especially the relation to conventional quantum field theories and the conditions under which conventional meson theories may be used as approximations need future clarification. The author hopes that this paper may stimulate such investigations.

REFERENCES

1. Bohm, D. Phys. Rev. 84: 166, 180. 1952.
2. Dirac, P. A. M. Proc. Roy. Soc. (London), A, 209: 291. 1951.
3. Heisenberg, W. Die physikalischen Prinzipien der Quantentheorie. Leipzig. 1930. p. 109.
4. Heisenberg, W. and Pauli, W. Z. Physik, 56: 1. 1929.
5. Kaempffer, F. A. Can. J. Phys. 31: 497, 629. 1953.
6. Kaempffer, F. A. Can. J. Phys. 31: 165. 1953.
7. Kramers, H. A. Physica, 18: 653. 1952.
8. Takabayasi, T. Progr. Theoret. Phys. (Japan), 9: 187. 1953.
9. Ziman, J. M. Proc. Roy. Soc. (London), A, 219: 257. 1953.

NOTE ON THE SELF-ENERGY OF SINGLE ROTON STATES IN QUANTUM HYDRODYNAMICS

By F. A. Kaempffer

It seems pretty well established, especially since Ziman (2) succeeded in giving Landau's (1) quantum hydrodynamics a sound foundation, that the peculiar behavior of liquid He II can be described in terms of excitations of the motion of the underlying liquid, called phonons and rotons, which appear upon quantization of the classical field equations of a nonviscous fluid, and which are characterized by a Hamiltonian the essential parts of which are

$$[1]\quad \mathfrak{H}_{\text{phonon}} = \tfrac{1}{2}\hbar c_0 \sum_{\mathbf{k}} k(a^*_{\mathbf{k}} a_{\mathbf{k}} + a_{\mathbf{k}} a^*_{\mathbf{k}}),$$

$$[2]\quad \mathfrak{H}_{\text{interaction}} = -\frac{i\hbar}{2}\sqrt{\frac{c_0\hbar}{2\rho_0 V}}\sum_{\mathbf{k}}\sum_{\mathbf{l}}\frac{(\mathbf{k}\cdot\mathbf{l})}{\sqrt{k}} \times (a_{\mathbf{k}} b^*_{\mathbf{l}+\mathbf{k}} b_{\mathbf{l}} + a_{\mathbf{k}} b^*_{\mathbf{l}} b_{\mathbf{l}-\mathbf{k}} + a^*_{-\mathbf{k}} b^*_{\mathbf{l}+\mathbf{k}} b_{\mathbf{l}} + a^*_{-\mathbf{k}} b^*_{\mathbf{l}} b_{\mathbf{l}-\mathbf{k}}),$$

$$[3]\quad \mathfrak{H}_{\text{roton}} = \frac{\hbar^2}{8\rho_0 V}\Big\{\sum_{\mathbf{k}}\sum_{\mathbf{l}}\sum_{\mathbf{m}}\sum_{\mathbf{n}}\delta_{\mathbf{k}+\mathbf{l},\mathbf{m}+\mathbf{n}}[(\mathbf{k}+\mathbf{n})\cdot(\mathbf{l}+\mathbf{m})]\, b^*_{\mathbf{m}} b^*_{\mathbf{n}} b_{\mathbf{k}} b_{\mathbf{l}} + \sum_{\mathbf{k}}\sum_{\mathbf{l}}(k^2+l^2)\, b^*_{\mathbf{k}} b_{\mathbf{k}}\Big\},$$

where $a^*_{\mathbf{k}}$, $a_{\mathbf{k}}$ and $b^*_{\mathbf{k}}$, $b_{\mathbf{k}}$ are the well-known creation and annihilation operators for phonons and rotons respectively, c_0 is the velocity of sound, ρ_0 the average density of the liquid, and $V = L_0^3$ is the normalization volume. Denoting by $|\, 1_{\mathbf{n}};\, N_{\mathbf{k}}\rangle$ a state of the liquid in which one roton of momentum $\hbar\mathbf{n}$ and N phonons of momentum $\hbar\mathbf{k}$ are excited, there exists a representation in which $\mathfrak{H}_{\text{phonon}} + \mathfrak{H}_{\text{roton}}$ is diagonal:

$$[4]\quad E^{(0)}_{1\mathbf{n};N\mathbf{k}} \equiv \langle 1_{\mathbf{n}};\, N_{\mathbf{k}}\,|\,\mathfrak{H}_{\text{phonon}} + \mathfrak{H}_{\text{roton}}\,|\,1_{\mathbf{n}};\, N_{\mathbf{k}}\rangle = \hbar c_0 \sum_{\mathbf{k}} k(N_{\mathbf{k}} + \tfrac{1}{2}) + \frac{\hbar^2}{8\rho_0 V}\sum_{\mathbf{l}}(l^2 + n^2).$$

The substructure of the liquid, consisting of N atoms, is introduced, according to Ziman (2), by cutting off the summations in [4] at a maximum propagation vector $k_{\max} = (2\pi/L_0)\kappa_{\max}$ so that

$$[5]\quad \frac{4\pi}{3}\kappa^3_{\max} = 3N.$$

The contribution of a single roton state $|\, 1_{\mathbf{n}};\, 0\rangle$ to the energy of the system is then given by

$$[6]\quad E^{(0)}_{1\mathbf{n};0} = \Delta + \frac{\hbar^2 n^2}{2\mu}$$

with

[7] $$\Delta = 2\pi^{4/3}\left(\frac{9}{4}\right)^{5/3}\hbar^2\rho_0^{2/3}m^{-5/3};\quad \mu = \frac{4}{3}m;\quad m = \frac{\rho_0 V}{N}$$

where "rest energy" Δ and "mass" μ of a roton have for liquid He II the numerical values

[8] $$\Delta/k \sim 7^\circ\,\mathrm{K.};\quad \mu = \frac{4}{3}(\text{mass of He-atom}).$$

It is the purpose of this note to investigate the contribution of the roton–phonon interaction $\mathfrak{H}_{\mathrm{int}}$ to the energy of a single roton state and to show, if $\mathfrak{H}_{\mathrm{int}}$ is treated as a perturbation,

(1) that the numerical values [8] are not trustworthy, since $\mathfrak{H}_{\mathrm{int}}$ contributes to the energy in second approximation a term of the same order of magnitude as $E^{(0)}$, and

(2) that the tendency of $\mathfrak{H}_{\mathrm{int}}$ would be to decrease the numerical value of Δ considerably and to leave the value of μ practically unchanged in the case of liquid He II.

Clearly, if $\mathfrak{H}_{\mathrm{int}}$ is treated as a perturbation, with $\mathfrak{H}_{\mathrm{phonon}} + \mathfrak{H}_{\mathrm{roton}}$ as unperturbed Hamiltonian, it will not contribute in first approximation to the energy of single roton states:

[9] $$E^{(1)}_{1_{\mathbf{n}};0} \equiv \langle 1_{\mathbf{n}};0 \mid \mathfrak{H}_{\mathrm{int}} \mid 1_{\mathbf{n}};0\rangle = 0$$

because $\mathfrak{H}_{\mathrm{int}}$ is linear in the phonon creation and annihilation operators $a^*_{\mathbf{k}}$, $a_{\mathbf{k}}$. This will be true even with an arbitrary number $N_{\mathbf{k}}$ of phonons present. In second approximation, however, there will be a contribution

[10] $$E^{(2)}_{1_{\mathbf{n}};0} = \sum_{\mathbf{k}} \frac{\langle 1_{\mathbf{n}};0 \mid \mathfrak{H}_{\mathrm{int}} \mid 1_{\mathbf{n}+\mathbf{k}};1_{-\mathbf{k}}\rangle\langle 1_{\mathbf{n}+\mathbf{k}};1_{-\mathbf{k}} \mid \mathfrak{H}_{\mathrm{int}} \mid 1_{\mathbf{n}};0\rangle}{E^{(0)}_{1_{\mathbf{n}};0} - E^{(0)}_{1_{\mathbf{n}+\mathbf{k}};1_{-\mathbf{k}}}}$$

describing the fact that the roton of momentum $\mathbf{n}$ will spend part of its life in excited states of momentum $\mathbf{n}+\mathbf{k}$ between emission and reabsorption of a virtual phonon momentum $-\mathbf{k}$. One may therefore call this term appropriately the "self-energy" of a single roton state. The evaluation of [10] is straightforward; one has

[11] $$E^{(0)}_{1_{\mathbf{n}};0} = \Delta + \frac{\hbar^2 n^2}{2\mu};\quad E^{(0)}_{1_{\mathbf{n}+\mathbf{k}};1_{-\mathbf{k}}} = \Delta + \frac{\hbar^2}{2\mu}(\mathbf{n}+\mathbf{k})^2 + \hbar c_0 k,$$

[12] $$\langle 1_{\mathbf{n}+\mathbf{k}};1_{-\mathbf{k}} \mid \mathfrak{H}_{\mathrm{int}} \mid 1_{\mathbf{n}};0\rangle = \langle 1_{\mathbf{n}};0 \mid \mathfrak{H}_{\mathrm{int}} \mid 1_{\mathbf{n}+\mathbf{k}};1_{-\mathbf{k}}\rangle^* = -\frac{\hbar i}{2}\sqrt{\frac{c_0\hbar}{2\rho_0 V}}\left(\frac{2(\mathbf{k}\cdot\mathbf{n}) + k^2}{\sqrt{k}}\right),$$

and obtains, after converting the summation over $\mathbf{k}$ into an integration,

[13] $$E^{(2)}_{1_{\mathbf{n}};0} = \frac{-\beta}{2\kappa_{\max}^4}\Delta\int_0^{\kappa_{\max}}\int_{-1}^{+1}\frac{(2\kappa\nu z + \kappa^2)^2\,dz\,d\kappa}{(2\nu z + \kappa + \beta\kappa_{\max})}$$

with $\kappa = (L_0/2\pi)k$; $\nu = (L_0/2\pi)n$, and $L_0\mu c_0/\pi\hbar = \beta\kappa_{\max}$, where

[14] $$\beta = \frac{4}{3\pi}\left(\frac{9}{4\pi}\right)^{1/3}\rho_0^{-1/3}m^{4/3}c_0\hbar^{-1}.$$

For liquid He II $\beta \cong 2$. The integral is elementary; expanding the result in powers of ν one obtains:

$$[15] \quad E^{(2)}_{1n;0} = -\Delta\left\{\beta^5 \ln\left(\frac{\beta+1}{\beta}\right) - \beta^4 + \beta^3 - \tfrac{1}{2}\beta^2 + \frac{1}{8}\beta\right\} - \left(\frac{9}{\pi}\right)^{4/3} 4^{-1/3}\left\{\beta^3 \ln\left(\frac{\beta+1}{\beta}\right) - \frac{\beta^3(2\beta+3)}{2(\beta+1)^2}\right\}\frac{\hbar^2 n^2}{2\mu} + O(n^4).$$

If one writes now the energy of a single roton state in the form

$$[16] \quad E_{1n;0} = E^{(0)}_{1n;0} + E^{(2)}_{1n;0} = \Delta' + \frac{\hbar^2 n^2}{2\mu'} + O(n^4),$$

one gets in the case of liquid He II ($\beta = 2$) the numerical values:

$$[17] \quad \Delta' \cong -2\Delta; \quad \mu' \cong \mu.$$

This result indicates clearly that the numerical value for Δ obtained from the diagonalization of $\mathfrak{H}_{\text{roton}}$ alone is quite unreliable, and moreover, that the "corrected" values [17] cannot be trusted either, because the phonon–roton interaction is the main contributor to the rest energy of the roton, which appears to be caused mainly by processes of the self-energy type. It must be concluded that any attempt at diagonalization of the Hamiltonian [1], [2], [3] is unlikely to be successful, if $\mathfrak{H}_{\text{phonon}} + \mathfrak{H}_{\text{roton}}$ is taken as the unperturbed part of the Hamiltonian, since $\mathfrak{H}_{\text{int}}$ cannot be considered as small in the sense of perturbation theory.

The author is indebted to Mr. E. Lokken for valuable comments.

1. LANDAU, L. D. J. Phys. U.S.S.R. 5: 71. 1941.
2. ZIMAN, J. M. Proc. Roy. Soc. (London), A, 219: 257. 1953.

RECEIVED DECEMBER 16, 1953.
DEPARTMENT OF PHYSICS,
UNIVERSITY OF BRITISH COLUMBIA,
VANCOUVER 8, B.C.

CANADIAN JOURNAL OF PHYSICS

Notes to Contributors

Manuscripts

(i) ***General.*** Manuscripts should be typewritten, double spaced, on paper 8½×11 in. **The original and one copy are to be submitted.** Tables (each typed on a separate sheet) and captions for the figures should be placed at the end of the manuscript. Every sheet of the manuscript should be numbered.

Style, arrangement, spelling, and abbreviations should conform to the usage of this journal. Names of all simple compounds, rather than their formulas, should be used in the text. Greek letters or unusual signs should be written plainly or explained by marginal notes. Superscripts and subscripts must be legible and carefully placed.

Manuscripts should be carefully checked before they are submitted; authors will be charged for changes made in the proof that are considered excessive.

(ii) ***Abstract.*** An abstract of not more than about 200 words, indicating the scope of the work and the principal findings, is required, except in Notes.

(iii) ***References.*** References should be listed **alphabetically by authors' names,** numbered, and typed after the text. The form of the citations should be that used in this journal; in references to papers in periodicals, titles should not be given and only initial page numbers are required. All citations should be checked with the original articles and each one referred to in the text by the key number.

(iv) ***Tables.*** Tables should be numbered in roman numerals and each table referred to in the text. Titles should always be given but should be brief; column headings should be brief and descriptive matter in the tables confined to a minimum. Numerous small tables should be avoided.

Illustrations

(i) ***General.*** All figures (including each figure of the plates) should be numbered consecutively from 1 up, in arabic numerals, and each figure referred to in the text. The author's name, title of the paper, and figure number should be written in the lower left corner of the sheets on which the illustrations appear. Captions should not be written on the illustrations (see Manuscript (i)).

(ii) ***Line Drawings.*** Drawings should be carefully made with India ink on white drawing paper, blue tracing linen, or co-ordinate paper ruled in blue only; any co-ordinate lines that are to appear in the reproduction should be ruled in black ink. Paper ruled in green, yellow, or red should not be used unless it is desired to have all the co-ordinate lines show. All lines should be of sufficient thickness to reproduce well. Decimal points, periods, and stippled dots should be solid black circles large enough to be reduced if necessary. Letters and numerals should be neatly made, preferably with a stencil (**do NOT use typewriting**), and be of such size that the smallest lettering will be not less than 1 mm. high when reproduced in a cut 3 in. wide.

Many drawings are made too large; originals should not be more than 2 or 3 times the size of the desired reproduction. In large drawings or groups of drawings the ratio of height to width should conform to that of a journal page but the height should be adjusted to make allowance for the caption.

The original drawings and one set of clear copies (e.g. small photographs) are to be submitted.

(iii) ***Photographs.*** Prints should be made on glossy paper, with strong contrasts. They should be trimmed so that essential features only are shown and mounted carefully, with rubber cement, on white cardboard.

As many photographs as possible should be mounted together (with a **very** small space between each photo) to reduce the number of cuts required. Full use of the space available should be made and the ratio of height to width should correspond to that of a journal page; however, allowance must be made for the captions. Photographs or groups of photographs should not be more than 2 or 3 times the size of the desired reproduction.

Photographs are to be submitted in duplicate; if they are to be reproduced in groups one set should be mounted, the duplicate set unmounted.

Reprints

A total of 50 reprints of each paper, without covers, are supplied free. Additional reprints, with or without covers, may be purchased.

Charges for reprints are based on the number of printed pages, which may be calculated approximately by multiplying by 0.6 the number of manuscript pages (double-spaced typewritten sheets, 8½ × 11 in.) and making allowance for illustrations (not inserts). The cost per page is given on the reprint requisition which accompanies the galley.

Any reprints required in addition to those requested on the author's reprint requisition form must be ordered officially as soon as the paper has been accepted for publication.

Contents

Page

The Impedance of an Antenna above a Circular Ground Plate Laid upon a Plane Earth—*G. Bekefi* - - - - - - - - - - - - - 205

The Radioactive Isotopes Al^{24}, P^{28}, Cl^{32}—*S. W. Breckon, A. Henrikson, W. M. Martin, and J. S. Foster* - - - - - - - - - - - - 223

Fine Structure of the $F^{19}(\gamma, n)F^{18}$ Activation Curve—*J. G. V. Taylor, L. B. Robinson, and R. N. H. Haslam* - - - - - - - - - - 238

Refractive Index Nomogram for Dry and Humid Air—*P. A. Bricout* 243

The Emission Spectrum of Aluminum Monofluoride. II—*S. M. Naudé and T. J. Hugo* - - - - - - - - - - - - - - - - - 246

On the Concept of Field Quantization—*F. A. Kaempffer* - - - - 259

Note on the Self-energy of Single Roton States in Quantum Hydrodynamics—*F. A. Kaempffer* - - - - - - - - - - - - - - 264

Printed in Canada *by* University of Toronto Press